Time-odd mean fields in covariant density functional theory: Nonrotating systems

A. V. Afanasjev[*] and H. Abusara

Department of Physics and Astronomy, Mississippi State University, Mississippi State, Mississippi 39762, USA

(Received 25 March 2009; revised manuscript received 9 October 2009; published 20 January 2010)

Time-odd mean fields (nuclear magnetism) are analyzed in the framework of covariant density functional theory (CDFT) by blocking the single-particle states with a fixed signature. It is shown that they always provide additional binding to the binding energies of odd-mass nuclei. This additional binding only weakly depends on the relativistic mean-field parametrization, reflecting good localization of the properties of time-odd mean fields in CDFT. The underlying microscopic mechanism is discussed in detail. Time-odd mean fields affect odd-even mass differences. However, our analysis suggests that the modifications of the strength of pairing correlations required to compensate for their effects are modest. In contrast, time-odd mean fields have a profound effect on the properties of odd-proton nuclei in the vicinity of the proton drip line. Their presence can modify the half-lives of proton emitters (by many orders of magnitude in light nuclei) and considerably affect the possibilities of their experimental observation.

DOI: 10.1103/PhysRevC.81.014309 PACS number(s): 21.60.Jz, 21.10.Dr, 21.10.Pc, 27.40.+z

I. INTRODUCTION

The development of self-consistent many-body theories aiming at the description of low-energy nuclear phenomena provides the necessary theoretical tools for an exploration of the nuclear chart into known and unknown regions. Theoretical methods (both relativistic and nonrelativistic) formulated within the framework of density functional theory (DFT) and effective field theory (EFT) are the most promising tools for the global investigation of the properties of atomic nuclei. The DFT and EFT concepts in nuclear structure models have been extensively discussed in a number of recent articles [1–4]. The power of the models based on these concepts is essentially unchallenged in medium- and heavy-mass nuclei, where *ab initio*-type few-body calculations are computationally impossible and the applicability of the spherical shell model is restricted to a few regions in the vicinity of double shell closures.

The self-consistent mean-field approach to nuclear structure represents an approximate implementation of the Kohn-Sham DFT [5–8], which is successfully employed in the treatment of the quantum many-body problem in atomic, molecular, and condensed matter physics. The DFT enables a description of the nuclear many-body problem in terms of energy density functionals (EDFs), and self-consistent mean-field models approximate these functionals, which include all higher-order correlations, with powers and gradients of ground-state nucleon densities (see Refs. [3] and [9–12] and references therein). EDFs are universal in the sense that they can be applied to nuclei all over the periodic table. Although they model the effective interaction between nucleons, EDFs are not necessarily related to any nucleon-nucleon (NN) potential. By employing these energy functionals, adjusted to reproduce the empirical properties of symmetric and asymmetric nuclear matter, and bulk properties of some spherical nuclei, the current generation of self-consistent mean-field methods has achieved a high level of accuracy in the description of ground states and properties of excited states in arbitrarily heavy nuclei, exotic nuclei far from β stability, and nuclear systems at the nucleon drip lines (see Refs. [10], [11], and [13] and references therein).

Self-consistent methods (such as Hartree-Fock and Hartree-Fock-Bogoliubov) based on zero-range Skyrme forces or finite-range Gogny forces are frequently used in nuclear structure calculations [10,14]. These approaches represent nonrelativistic EDFs based on the Schrodinger equation for the many-body nuclear problem [10].

On the other hand, one can formulate the class of relativistic models based on the Dirac formalism, which can generally be defined as *covariant density functionals* (CDFs) [11]. These models, such as quantum hadrodynamics [9,15], are based on concepts of nonrenormalizable effective relativistic field theories and DFTs, and they provide a very interesting relativistic framework for studies of nuclear structure phenomena at and far from the valley of β-stability [11]. Relativistic mean-field (RMF) models [15] are analogs of the Kohn-Sham formalism of the DFT [7], with local scalar and vector fields appearing in the role of local relativistic Kohn-Sham potentials [1,9]. The EDF is approximated with the powers and gradients of auxiliary meson fields or nucleon densities. The EFT building of the EDT allows error estimates to be made, provides a power counting scheme that separates long- and short-distance dynamics, and, therefore, removes model dependences from the self-consistent mean field approach [16]. In the description of nuclear ground states and the properties of excited states the self-consistent mean-field implementations of quantum hadrodynamics, the relativistic Hartree-Bogoliubov (RHB) model, and the relativistic (quasiparticle) random phase approximation, and their subversions, are employed [11].

The *mean field* is a basic concept of every DFT. One can specify *time-even* and *time-odd* mean fields [17,18], dependent on the response of these fields to the action of a time-reversal operator. The properties of time-even mean fields in nuclear density functionals are reasonably well understood and defined [10,11]. This is because (i) many physical observables such as

[*]afansjev@erc.msstate.edu

binding energies and radii are sensitive only to these fields, and (ii) the model parameters are fitted to such physical observables.

On the other hand, the properties of time-odd mean fields, which appear only in nuclear systems with broken time-reversal symmetry, are still poorly understood. However, it is already known that these fields are important for proper description of rotating nuclei [17–21], band terminations [22,23], magnetic moments [24], isoscalar monopole vibrations [25], electric giant resonances [26], high-amplitude collective dynamics [27], fusion process [28], the strengths and energies of Gamow-Teller resonances [29], the binding energies of odd-mass nuclei [30–32], and the additivity of angular momentum alignments [33]. They also may play a role in $N = Z$ nuclei [30,34] and affect the definition of the strength of pairing correlations [32,35].

There was a dedicated effort to better understand time-odd mean fields in the framework of the Skyrme EDF theory (see Refs. [17,19,22,29] and references therein). On the contrary, much less attention has been paid to these fields in covariant density functional theory (CDFT) [18,24,32,35]. This is because time-odd mean fields are defined through the Lorentz invariance in the CDFT [11], and thus they do not require additional coupling constants. On the other hand, time-odd mean fields are not well defined in nonrelativistic DFTs [17,29], and as a consequence, there are a number of open questions related to these fields. The current article aims for a better and systematic understanding of time-odd mean fields and their impact on physical observables in nonrotating nuclei in the framework of the RMF realization of the CDFT. The results of the study of these fields in rotating nuclei will be presented in a forthcoming article [36] that represents a continuation of the current investigation.

The paper is organized as follows. The cranked RMF theory and its details related to time-odd mean fields are discussed in Sec. II. Section III is devoted to the analysis of the impact of time-odd mean fields on binding energies of odd-mass nuclei. The mass and particle number dependences of this impact and their connections with odd-even mass staggerings are also considered. The microscopic mechanism of additional binding in odd-mass nuclei induced by time-odd mean fields is analyzed in Sec. IV. The impact of time-odd mean fields on the properties of proton-unstable nuclei is studied in Sec. V. Section VI considers how time-odd mean fields modify the properties of odd-odd nuclei. Finally, Sec. VII reports the main conclusions of our work.

II. THEORETICAL FORMALISM

The results presented in the current article were obtained using the cranked relativistic mean field (CRMF) theory [21,37,38]. This theory has been successfully employed for the description of rotating nuclei (see Ref. [39] and references therein) in which the time-odd mean fields play an important role, but it is also able to describe nuclear systems with broken time-reversal symmetry in the intrinsic frame at no rotation. In this theory pairing correlations are neglected, which allows better isolation of the effects induced by time-odd mean fields. The CRMF computer code is formulated in the signature basis. As a result, the breaking of Kramer's degeneracy of single-particle states is taken into account in a fully self-consistent way. This is important for an accurate description of time-odd mean fields in fermionic channels (see Sec. IV). The most important features of the CRMF formalism related to time-odd mean fields are outlined here (for more details see Refs. [37] and [38]) for the case of no rotation (rotational frequency $\Omega_x = 0$).

In the Hartree approximation, the stationary Dirac equation for nucleons in the intrinsic frame is given by

$$\hat{h}_D \psi_i = \varepsilon_i \psi_i, \tag{1}$$

where $\hat{h}_D$ is the Dirac Hamiltonian for a nucleon with mass m:

$$\hat{h}_D = \boldsymbol{\alpha}[-i\nabla - \boldsymbol{V}(\boldsymbol{r})] + V_0(\boldsymbol{r}) + \beta[m + S(\boldsymbol{r})]. \tag{2}$$

It contains the average fields determined by the mesons, that is, the attractive scalar field $S(\mathbf{r})$,

$$S(\boldsymbol{r}) = g_\sigma \sigma(\boldsymbol{r}), \tag{3}$$

and the repulsive time-like component of the vector field $V_0(\boldsymbol{r})$,

$$V_0(\boldsymbol{r}) = g_\omega \omega_0(\boldsymbol{r}) + g_\rho \tau_3 \rho_0(\boldsymbol{r}) + e\frac{1-\tau_3}{2} A_0(\boldsymbol{r}). \tag{4}$$

A magnetic potential $\boldsymbol{V}(\boldsymbol{r})$,

$$\boldsymbol{V}(\boldsymbol{r}) = g_\omega \boldsymbol{\omega}(\boldsymbol{r}) + g_\rho \tau_3 \boldsymbol{\rho}(\boldsymbol{r}) + e\frac{1-\tau_3}{2} \boldsymbol{A}(\mathbf{r}), \tag{5}$$

originates from the space-like components of the vector mesons. Note that in these equations, the four-vector components of the vector fields ω^μ, ρ^μ, and A^μ are separated into time-like (ω_0, ρ_0, and A_0) and space-like [$\boldsymbol{\omega} = (\omega^x, \omega^y, \omega^z)$, $\boldsymbol{\rho} = (\rho^x, \rho^y, \rho^z)$, and $\boldsymbol{A} = (A^x, A^y, A^z)$] components. In the Dirac equation the magnetic potential has the structure of a magnetic field. Therefore the effect produced by it is called *nuclear magnetism* (NM) [37].

The corresponding meson fields and the electromagnetic potential are determined by the Klein-Gordon equations,

$$\begin{aligned}
\{-\Delta + m_\sigma^2\}\sigma(\boldsymbol{r}) &= -g_\sigma\left[\rho_s^n(\boldsymbol{r}) + \rho_s^p(\boldsymbol{r})\right] \\
&\quad - g_2\sigma^2(\boldsymbol{r}) - g_3\sigma^3(\boldsymbol{r}), &(6)\\
\{-\Delta + m_\omega^2\}\omega_0(\boldsymbol{r}) &= g_\omega\left[\rho_v^n(\boldsymbol{r}) + \rho_v^p(\boldsymbol{r})\right], &(7)\\
\{-\Delta + m_\omega^2\}\boldsymbol{\omega}(\boldsymbol{r}) &= g_\omega[\boldsymbol{j}^n(\boldsymbol{r}) + \boldsymbol{j}^p(\boldsymbol{r})] &(8)\\
\{-\Delta + m_\rho^2\}\rho_0(\boldsymbol{r}) &= g_\rho\left[\rho_v^n(\boldsymbol{r}) - \rho_v^p(\boldsymbol{r})\right], &(9)\\
\{-\Delta + m_\rho^2\}\boldsymbol{\rho}(\boldsymbol{r}) &= g_\rho[\boldsymbol{j}^n(\boldsymbol{r}) - \boldsymbol{j}^p(\boldsymbol{r})], &(10)\\
-\Delta A_0(\boldsymbol{r}) = e\rho_v^p(\boldsymbol{r}), &\quad -\Delta \boldsymbol{A}(\boldsymbol{r}) = e\boldsymbol{j}^p(\boldsymbol{r}), &(11)
\end{aligned}$$

with source terms involving the various nucleonic densities and currents,

$$\rho_s^{n,p}(\boldsymbol{r}) = \sum_{i=1}^{N,Z} [\psi_i(\boldsymbol{r})]^\dagger \hat{\beta} \psi_i(\boldsymbol{r}), \tag{12}$$

$$\rho_v^{n,p}(\boldsymbol{r}) = \sum_{i=1}^{N,Z} [\psi_i(\boldsymbol{r})]^\dagger \psi_i(\boldsymbol{r}), \tag{13}$$

$$\boldsymbol{j}^{n,p}(\boldsymbol{r}) = \sum_{i=1}^{N,Z} [\psi_i(\boldsymbol{r})]^\dagger \hat{\boldsymbol{\alpha}} \psi_i(\boldsymbol{r}), \tag{14}$$

where the labels n and p are used for neutrons and protons, respectively. In these equations, the sums run over the occupied positive-energy shell model states only (*no-sea approximation*) [15,40]. Note that the spatial components of the vector potential $\boldsymbol{A}(\boldsymbol{r})$ are neglected in the calculations because the coupling constant of the electromagnetic interaction is small compared with the coupling constants of the meson fields.

The magnetic potential $\boldsymbol{V}(\boldsymbol{r})$ in the Dirac equation as well as the currents $\boldsymbol{j}^{n,p}(\boldsymbol{r})$ in the Klein-Gordon equations do not appear in the RMF equations for time-reversal systems [15]. Similarly to the nonrelativistic case, their presence leads to the appearance of time-odd mean fields. Thus, we use the terms *nuclear magnetism* and *time-odd mean fields* interchangeably throughout this article. The magnetic potential is the contribution to the mean field that breaks time-reversal symmetry in the intrinsic frame and induces nonvanishing currents $\boldsymbol{j}^{n,p}$ [Eq. (14)] in the Klein-Gordon equations [Eqs. (8) and (10)], which are related to the space-like components of the vector mesons. In turn, the space-like components of the vector $\boldsymbol{\omega}$ and $\boldsymbol{\rho}$ fields form the magnetic potential (5) in the Dirac equation. Note that the current $\boldsymbol{j}^{n,p}(\boldsymbol{r})$ changes sign upon the action of the time-reversal operator [41]. Together with densities it forms the covariant four-vector $j^\mu = \{\rho, \boldsymbol{j}\}$. As a consequence, these two quantities (ρ and $\boldsymbol{j}$) do not transform independently under Lorentz transformation. This explains why the structure of the Klein-Gordon equations for time-like and space-like components of vector mesons is the same [compare, e.g., Eqs. (7) and (8) for ω mesons] and why the same coupling constant stands in front of the densities and currents on the right-hand side of these equations.

The spatial components of the vector ω and ρ mesons lead to the interactions between possible currents. For the ω meson this interaction is attractive for all combinations (pp, nn, and pn currents), and for the ρ meson it is attractive for pp and nn currents but repulsive for pn currents. Within mean field theory such currents occur only in the situations of broken time-reversal symmetry.

Note that time-odd mean fields related to NM are defined through the Lorentz invariance [11] and thus they do not require additional coupling constants: the coupling constants of time-even mean fields are used also for time-odd mean fields.

The currents are isoscalar and isovector in nature for ω and ρ mesons [Eqs. (8) and (10)], respectively. As a consequence, the contribution of the ρ meson to the magnetic potential and total energy is marginal in the majority of cases even at the neutron drip line (see Sec. IV B for details). Thus, time-odd mean fields in the RMF framework depend predominantly on the spatial components of the ω meson. Neglecting the contribution of the ρ meson, one can see that only two parameters, namely, the mass m_ω and coupling constant g_ω of the ω meson, define the properties of time-odd mean fields [Eqs. (5), (8), and (10)]. Figure 1 clearly indicates that these parameters are well localized in the parameter space for parametrizations of the RMF Lagrangian in groups A, B, and C (see caption to Fig. 1 for group definitions). This suggests that the parameter dependence of the impact of time-odd mean fields on physical observables should be quite weak for these types of parametrizations. Indeed, the analysis of terminating states in Ref. [23] showed that time-odd mean fields are defined with an accuracy of about 15% for parametrizations of the RMF Lagrangian containing only nonlinear self-couplings for the σ meson (group A).

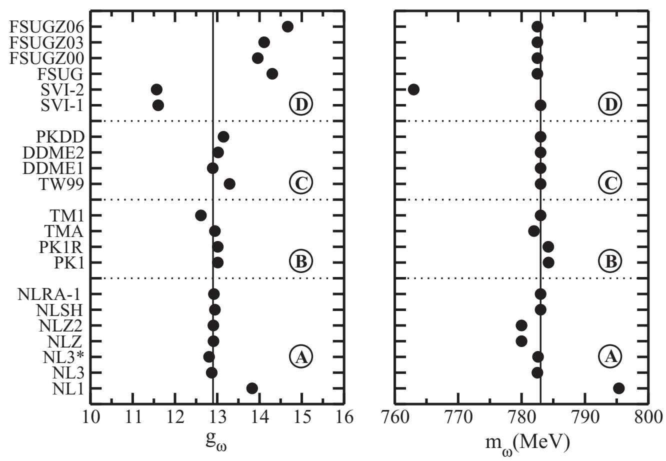

FIG. 1. The m_ω and g_ω parameters of different modern parametrizations of the RMF Lagrangian. They are combined into four groups, dependent on how self- and mixed couplings are introduced. Group A represents parametrizations that include nonlinear self-couplings only for the σ meson. Group B contains parametrizations that include self-couplings for σ and ω mesons (and ρ mesons in the case of PK1R). Group C represents parametrizations that include density-dependent meson-nucleon couplings for σ, ω, and ρ mesons. The other parametrizations are included in group D. SVI and SVI-2 parametrizations neglect nonlinear self-couplings for the σ meson but include isoscalar-isovector couplings. The other parametrizations in group D include mixed interaction terms (such as isoscalar-isovector couplings [52]) in addition to nonlinear self-couplings for the σ meson. Parameters are taken from Refs. [40] (NL1), [42] (NL3), [43] (NL3*), [44] (NLZ), [45] (NLZ2), [47] (NLSH), [46] (NLRA-1), [48] (PK1,PK1R), [49] (TMA), [50] (TM1), [51] (SVI1,SVI-2), [52] (FSUGold), [53] (FSUGZ00,FSUGZ03,FSUGZ06), [54] (TW99), [55] (DDME1), [56] (DDME2), and [48] (PKDD). Note that we omitted mass-dependent terms for g_ω in the TMA parametrization, which is a good approximation for heavy nuclei, as $g_\omega = 12.842 + 3.191A^{-0.4}$ [49].

On the other hand, Fig. 1 suggests that time-odd mean fields may be less accurately defined in parametrizations in group D, which include mixed interaction terms such as isoscalar-isovector couplings. However, it is premature to make such a conclusion because these parametrizations have not been tested extensively even on nuclear structure data sensitive to time-even mean fields. This is contrary to the parametrizations of groups A–C, which have successfully passed this test.

Investigation of all these parametrizations is definitely beyond the scope of this study. Thus, the present investigation focused on the study of time-odd mean fields in the CDFT with parametrizations of the RMF Lagrangian including only nonlinear self-couplings of the σ meson (group A parametrizations). The results of the study of time-odd mean fields in groups B–D parametrizations of meson-coupling models as well as within point-coupling models is presented in the forthcoming companion paper [36].

The total energy of the system is given in Refs. [37] and [38]. To facilitate the discussion we split it into different terms as[1]

$$E_{\rm tot} = E_{\rm part} + E_{\rm cm} - E_\sigma - E_{\sigma\rm NL} - E^{\rm TL}_\omega - E^{\rm TL}_\rho - E^{\rm SL}_\omega - E^{\rm SL}_\rho - E_{\rm Coul}, \tag{15}$$

where $E_{\rm part}$ and $E_{\rm cm}$ represent the contributions from fermionic degrees of freedom, whereas the other terms are related to mesonic (bosonic) degrees of freedom. In Eq. (15)

$$E_{\rm part} = \sum_i^A \varepsilon_i \tag{16}$$

is the energy of the particles moving in the field created by the mesons (ε_i is the energy of the ith particle and the sum runs over all occupied proton and neutron states),

$$E_\sigma = \frac{1}{2} g_\sigma \int d^3r\, \sigma(\boldsymbol{r})\left[\rho^p_s(\boldsymbol{r}) + \rho^n_s(\boldsymbol{r})\right] \tag{17}$$

is the linear contribution to the energy of the isoscalar-scalar σ field,

$$E_{\sigma\rm NL} = \frac{1}{2}\int d^3r \left[\frac{1}{3} g_2 \sigma^3(\boldsymbol{r}) + \frac{1}{2} g_3 \sigma^4(\boldsymbol{r})\right] \tag{18}$$

is the nonlinear contribution to the energy of the isoscalar-scalar σ field,

$$E^{\rm TL}_\omega = \frac{1}{2} g_\omega \int d^3r\, \omega_0(\boldsymbol{r})\left[\rho^p_v(\boldsymbol{r}) + \rho^n_v(\boldsymbol{r})\right] \tag{19}$$

is the energy of the time-like component of the isoscalar-vector ω field,

$$E^{\rm TL}_\rho = \frac{1}{2} g_\rho \int d^3r\, \rho_0(\boldsymbol{r})\left[\rho^n_v(\boldsymbol{r}) - \rho^p_v(\boldsymbol{r})\right] \tag{20}$$

is the energy of the time-like component of the isovector-vector ρ field,

$$E^{\rm SL}_\omega = -\frac{1}{2} g_\omega \int d^3r\, \boldsymbol{\omega}(\boldsymbol{r})[\boldsymbol{j}^p(\boldsymbol{r}) + \boldsymbol{j}^n(\boldsymbol{r})] \tag{21}$$

is the energy of the space-like component of the isoscalar-vector ω field,

$$E^{\rm SL}_\rho = -\frac{1}{2} g_\rho \int d^3r\, \boldsymbol{\rho}(\boldsymbol{r})[\boldsymbol{j}^n(\boldsymbol{r}) - \boldsymbol{j}^p(\boldsymbol{r})] \tag{22}$$

is the energy of the space-like component of the isovector-vector ρ field,

$$E_{\rm Coul} = \frac{1}{2} e \int d^3r\, A_0(\boldsymbol{r}) \rho^p_v(\boldsymbol{r}) \tag{23}$$

is the Coulomb energy, and

$$E_{\rm cm} = -\frac{3}{4}\hbar\omega_0 = -\frac{3}{4} 41 A^{-1/3} {\rm MeV} \tag{24}$$

is the correction for the spurious center-of-mass motion approximated by its value in a nonrelativistic harmonic oscillator potential.

The total energy of the system can alternatively be written as (similar to Refs. [57] and [58])

$$E_{\rm tot} = E_{\rm kin} + E_{\rm int} + E_{\rm cm}, \tag{25}$$

where the kinetic energy $E_{\rm kin}$ is given by

$$E_{\rm kin} = E_{\rm part} - 2(E_\sigma + E^{\rm TL}_\omega + E^{\rm TL}_\rho + E_{\rm Coul}), \tag{26}$$

and the interaction energy between nucleons $E_{\rm int}$ by

$$E_{\rm int} = E_\sigma + E^{\rm TL}_\omega + E^{\rm TL}_\rho + E_{\rm Coul} - E_{\sigma\rm NL} - E^{\rm SL}_\omega - E^{\rm SL}_\rho. \tag{27}$$

However, this representation of the total energy has a disadvantage compared with Eq. (15), as it does not provide direct access to the particle energy $E_{\rm part}$. The latter plays an important role in the understanding of the breaking of Kramer's degeneracy of time-reversal orbitals in the presence of time-odd mean fields (see Sec. IV A for details). Thus, further discussion of the total energy is based mostly on Eq. (15). However, we also provide the results of calculations for the kinetic energy $E_{\rm kin}$.

CRMF equations are solved in the basis of an anisotropic three-dimensional harmonic oscillator in Cartesian coordinates characterized by the deformation parameters $\beta_0 = 0.3$ ($\beta_0 = 0.4$ in the case of superdeformed states) and $\gamma = 0^\circ$ as well as the oscillator frequency $\hbar\omega_0 = 41A^{-1/3}$ MeV. Truncation of the basis is performed in such a way that all states belonging to shells up to fermionic $N_F = 12$ and bosonic $N_B = 16$ are taken into account in the calculations of light- and medium-mass nuclei. The fermionic basis is increased up to $N_F = 14$ in calculations of actinides. Numerical analysis indicates that this truncation scheme provides sufficient numerical accuracy for the physical quantities of interest.

Single-particle orbitals are labeled $[Nn_z\Lambda]\Omega^{\rm sign}$. $[Nn_z\Lambda]\Omega$ are the asymptotic quantum numbers (Nilsson quantum numbers) of the dominant component of the wave function. The "sign" superscripts to the orbital labels are sometimes used to indicate the sign of the signature r for that orbital ($r = \pm i$). The majority of the calculations are performed with the NL3 parametrization [42] of the RMF Lagrangian.

Many-particle configurations (hereafter, nuclear configurations or configurations) are specified by the occupation of available single-particle orbitals. In calculations without pairing, the occupation numbers n are integers ($n = 0$ or 1). In odd nuclei, all single-particle states with the exception of one are pairwise occupied. We call this occupied single-particle state of fixed signature, for which its time-reversal (signature) counterpart state is empty, the *blocked state* to simplify the discussion. The total signature and the parity of the configuration are the same as those of the blocked state. In the CRMF code, it is possible to specify the occupation of either the $r = +i$ or the $r = -i$ signature of the single-particle state. Specification of the nuclear configuration by means of listing all occupied single-particle states is impractical. Thus, we label the nuclear configuration in odd-mass nuclei by the Nilsson label and the signature of the blocked state. Note that

[1] We follow Refs. [57] and [58] in the selection of the signs of energy terms.

many physical observables, such as additional binding owing to NM, do not depend on the signature of the blocked state in odd-mass nuclei. In these cases, we omit the signature from the configuration label. In odd-odd nuclei, the Nilsson labels of the blocked proton and neutron states and their signatures are used for configuration labeling. Note that labeling by means of Nilsson labels is performed only when the calculated shape of the nuclear configuration is prolate or near-prolate.

To investigate the impact of NM (time-odd mean fields) on physical observables, CRMF calculations are performed in three calculational schemes for fixed configurations.

(i) Fully self-consistent calculations with NM included (hereafter denoted NM calculations),[2] which take into account spacelike components of the vector mesons [Eqs. (8), (10) and (5)], currents [Eqs. (8), (10), and (14)], and magnetic potential $\boldsymbol{V}(\boldsymbol{r})$ [Eq. (5).

(ii) Fully self-consistent calculations without NM (hereafter denoted WNM calculations),[3] which omit spacelike components of the vector mesons [Eqs. (8), (10) and (5)], currents [Eqs. (8), (10), and (14)], and magnetic potential $\boldsymbol{V}(\boldsymbol{r})$ [Eq. (5)]. Note that the results of the NM and WNM calculations are always compared for the same nuclear configuration.

(iii) Perturbative calculations (physical quantities of interest are indicated by the superscript "pert"). Fully self-consistent calculations with NM provide a starting point. Using their fields as input fields, only one iteration is performed in calculations without NM: this provides perturbative results. Time-even mean fields are the same in both (fully self-consistent and perturbative) calculations. Thus, the impact of time-odd mean fields on calculated quantities [e.g., different terms in the total energy; see Eq. (15)] is defined as the difference between the values of this quantity obtained in these two calculations. In this way, the pure effects of time-odd mean fields in fermionic and mesonic channels of the model are isolated because no polarization effects are introduced into time-even mean fields.

These are the ways in which the effects of time-odd mean fields can be studied, and as such they are frequently used in DFT studies, in both relativistic and nonrelativistic frameworks [17,18,21,23,24,30,31,59]. One should keep in mind, however, that if time-odd fields are neglected, the local Lorentz invariance (Galilean invariance in nonrelativistic frameworks [12,17]) is violated. The inclusion of time-odd mean fields restores the Lorentz invariance.

III. BINDING ENERGIES IN ODD-MASS NUCLEI

The time-reversal invariance is conserved in the ground states of even-even nuclei. The nucleon states are then pairwise degenerated, and the contribution of the state to the currents cancels with the contribution of its time-reversed partner. Time-odd mean fields reveal themselves in odd- and odd-odd mass nuclei and in two-(multi-)quasiparticle states of even-even nuclei. This is because an unpaired (odd) nucleon breaks the time-reversal invariance in the intrinsic frame and produces the contribution to the currents and spin. In this case, the Kramer's degeneracy of time-reversal partner orbitals is also broken.

Modifications of the binding energies and quasiparticle spectra are the most important issues when considering time-odd mean fields in nonrotating systems. Binding energies are important in nuclear astrophysics applications [60], and their modifications owing to time-odd mean fields may have considerable consequences for r- and rp-process abundances. Thus, it is important to understand the influence of time-odd mean fields on binding energies of odd- and odd-odd mass nuclei, especially in the context of mass table fits [61]. With the current focus on spectroscopic-quality DFT [62], knowledge of how time-odd mean fields influence the relative energies of different (quasi)particle states in model calculations is also needed.

Whereas there has been considerable interest in the study of time-odd mean fields in odd- and odd-odd mass nuclei at no rotation within the Skyrme EDF [30,31], relatively little is known about their role in the framework of the CDFT. So far, the impact of time-odd mean fields on binding energies has been studied in the CDFT framework only in odd-mass nuclei around doubly magic spherical nuclei [63] and in a few deformed nuclei around ^{32}S [64] and ^{254}No [32].

A. Binding energies in light nuclei

The impact of NM on the binding energies of light odd-mass nuclei is shown in Fig. 2. One can see that in all cases the presence of NM leads to additional binding, the magnitude of which is nucleus and state dependent. The absolute value of this additional binding is typically below 200 keV and only reaches 300 keV in some lower-mass nuclei. On average, the magnitude of additional binding owing to NM is inversely correlated with the mass of the nucleus; it is the largest in the lightest nuclei and the smallest in the heaviest nuclei. For each isotope chain, it is the largest in the vicinity of the proton drip line and the smallest in the vicinity of the neutron drip line. The polarization effects induced by NM and the energy splitting between the blocked state and its unoccupied signature partner induced by NM decrease with the increase in mass (compare Tables I and II below). This explains the observed trends in additional binding owing to NM.

[2]This method is equivalent to the Hartree-Fock method of Ref. [31].

[3]The difference between the WNM method of the present paper and the HFE method of Ref. [31] is only technical: it is related to the treatment of the occupation of the pair of energy degenerate states by an odd particle. The opposite signature states of this pair are occupied by an odd particle with probability 0.5 (in the filling approximation) in the HFE method (see Sec. IIC of Ref. [31]). On the contrary, one signature state of this pair is occupied with probability 1, whereas the other is empty, in the WNM method. However, time-reversal invariance is conserved in both approaches. This means that the Kramer's degeneracy of the single-particle levels is not violated and time-odd mean fields are not introduced into the system. As a consequence, if employed within the same framework, these two methods lead to the same results in calculations without pairing, as polarization and other effects induced by odd particles do not depend on the signature of the occupied state.

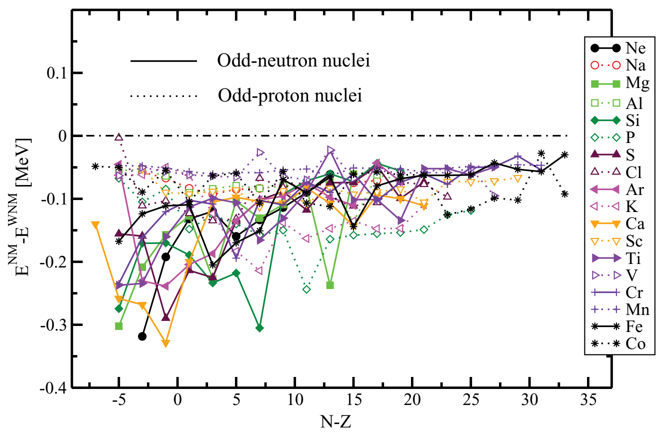

FIG. 2. (Color online) Impact of NM on binding energies of light odd-mass nuclei. Calculations were performed with the NL3 parametrization of the RMF Lagrangian. They cover nuclei from the proton drip line up to the neutron drip line.

Figure 3 shows that additional binding owing to NM only weakly depends on the RMF parametrization; this is also seen in the analysis of terminating states in Ref. [23]. In both cases, the largest deviation from the NL3 results is observed in the case of the NLSH parametrization.

It is interesting to compare these results with those obtained in the Skyrme EDF (see Fig. 4 in Ref. [30]). The modifications of total binding energy owing to time-odd mean fields are given by the quantity E^{to} in Ref. [30], which is an analog of the $E^{\mathrm{NM}} - E^{\mathrm{WNM}}$ quantity. The general dependence of both quantities on $N - Z$ is similar in odd-mass nuclei, apart from a few cases such as ^{43}Ti and ^{43}Sc in the SLy4 Skyrme EDF (Fig. 4 in Ref. [30]). Neither RMF nor Skyrme EDF calculations in odd-mass nuclei indicate the enhancement of time-odd mean fields in the vicinity of the $N = Z$ line. This is contrary to

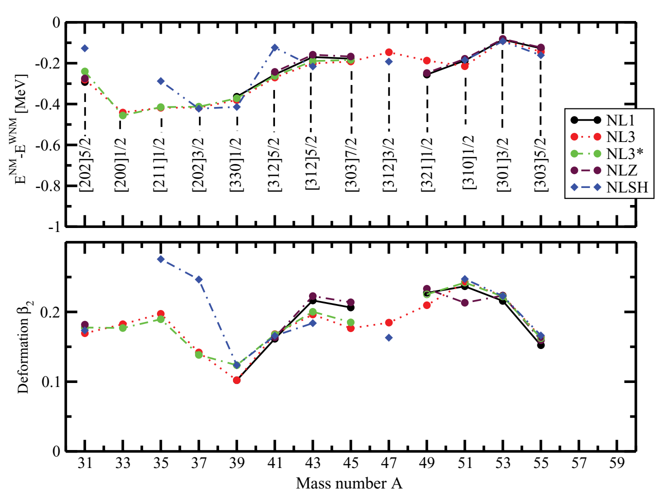

FIG. 3. (Color online) The same as Fig. 2 but for results obtained with the indicated parametrizations of the RMF Lagrangian in Ar isotopes. The structure of the ground states is shown by the Nilsson labels. Only when the structure of the ground state is the same as in the NL3 parametrization the results obtained with other parametrizations are shown.

Ref. [30], which suggested that the effects of time-odd mean fields are enhanced at the $N = Z$ line. The absolute values of the E^{to} and $E^{\mathrm{NM}} - E^{\mathrm{WNM}}$ quantities are similar, being below 300 keV in the majority of cases. The principal difference between the RMF and the Skyrme EDF lies in the fact that time-odd mean fields are always attractive and show very little dependence on parametrization in the RMF calculations (this is also supported by analysis of terminating states; see Ref. [23]), whereas they can be both attractive (SLy4 force) or repulsive (SIII force) and show considerable dependence on parametrization in the Skyrme EDF [30].

B. Binding energies in Ce ($Z = 58$) isotopes

The role of time-odd mean fields is studied here in medium-mass Ce isotopes to facilitate comparison with the results obtained within the Skyrme EDF with the SLy4 force in Ref. [31]. This reference represents the most detailed study of time-odd mean fields in odd-mass nuclei within the Skyrme EDF. We consider the lowest configurations of positive and negative parities, whereas Ref. [31] studies only the lowest configurations in each nucleus.

Figures 4 and 5 show the additional binding owing to NM. Comparison with the Skyrme EDF results in Ref. [31] reveals a number of important differences. First, similar to the results in light nuclei (Sec. III A) and in the actinide region (Sec. VI H in Ref. [32]), time-odd mean fields are attractive in RMF calculations for Ce isotopes. On the contrary, they are repulsive in the SLy4 parametrization of the Skyrme EDF [31]. Note that the SLy4 force produces attractive time-odd mean fields in light nuclei [30]. This mass dependence of the effects of time-odd mean fields in the Skyrme EDF may be because of the competition between isovector and isoscalar effects [31]. The average absolute magnitude of the change in binding owing to time-odd mean fields in RMF calculations is only half that seen in the Skyrme calculations with the SLy4 parametrization. It was also checked in some examples that additional binding owing to NM only weakly depends on the parametrization of the RMF Lagrangian.

Second, the results of the calculations do not reveal a strong dependence of additional binding owing to NM on deformation. For example, the deformation of the $\nu[615]11/2$ configuration in the $^{173-181}$Ce chain changes drastically from $\beta_2 \sim 0.23$ down to $\beta_2 \sim 0.06$ (Fig. 4, bottom panel), but the additional binding owing to NM remains almost the same (Fig. 4, top panel). The $\nu[523]7/2$ and $\nu[505]11/2$ configurations are other examples of this feature (Fig. 5).

Third, the binding energy modifications owing to time-odd mean fields are completely different in the RMF and Skyrme EDF calculations. In the Skyrme EDF calculations, the magnitude of these binding energy modifications is related to three properties of the blocked orbital. In decreasing order of importance, they are [31] a small Ω quantum number, a down-sloping behavior of the energy of the single-particle state with mass number A, and a large total angular momentum j for the spherical shell from which the single-particle state originates. For example, the binding energy modifications owing to time-odd mean fields will be larger for a configuration based on a blocked single-particle state with a small Ω than for a configuration with a large Ω of the blocked

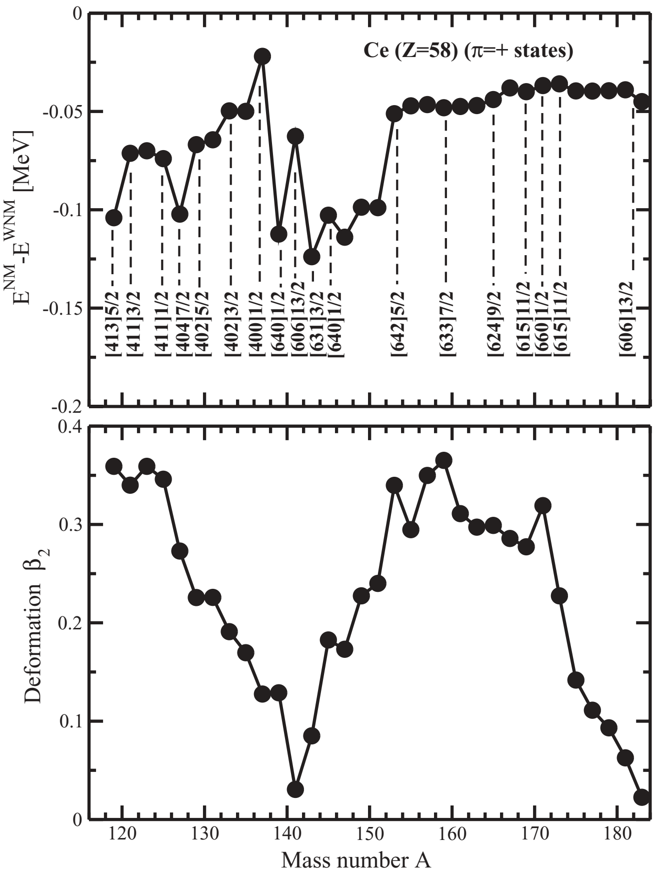

FIG. 4. Impact of NM on the binding energies of positive-parity configurations in odd-mass Ce ($Z = 58$) nuclei. The upper panel shows additional binding $E^{\rm NM} - E^{\rm WNM}$ owing to NM and its configuration dependence. Configurations are labeled with the Nilsson labels of the blocked states; configurations at and to the right of the Nilsson label up to the next Nilsson label have the same blocked state. The bottom panel shows the corresponding deformations of the configurations. Calculations were performed with the NL3 parametrization of the RMF Lagrangian. They cover nuclei from the proton drip line up to the neutron drip line.

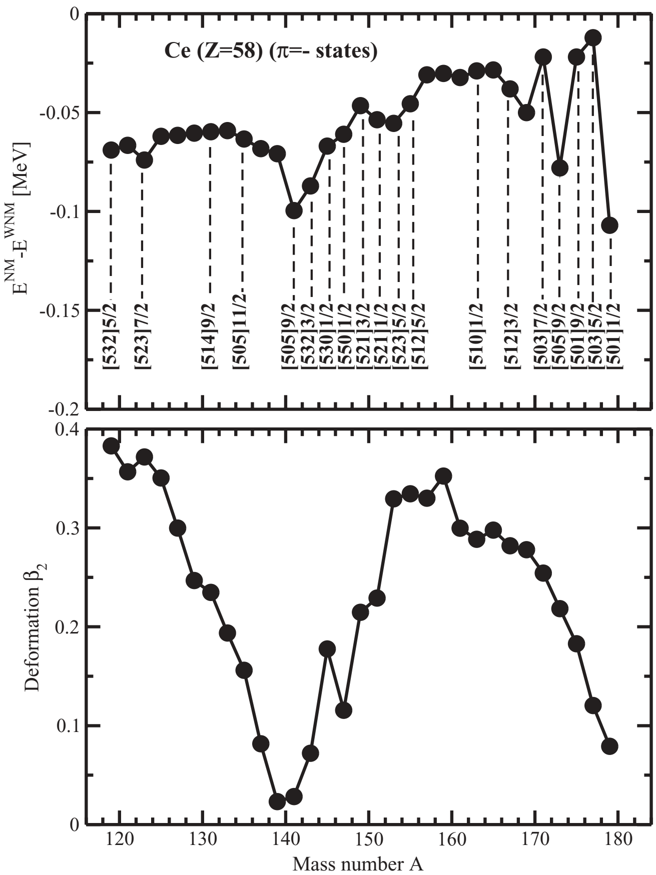

FIG. 5. The same as Fig. 4 but for negative-parity configurations.

state if both blocked states belong to the same j shell. On the contrary, RMF calculations do not reveal this type of correlation between additional binding owing to NM and the structure of the blocked state. Indeed, the configurations that have the largest changes in binding energies owing to NM ($|E^{\rm NM} - E^{\rm WNM}| \geqslant 0.1$ MeV) are [413]5/2, [404]7/2, [640]1/2, [631]3/2, [505]9/2, and [501]1/2.

C. Current distributions

When discussing current distributions, it is important to remember that calculations are performed in the one-dimensional cranking approximation. Although the rotational frequency is equal to zero in the calculations, the results for currents still obey the symmetries imposed by the cranking approximation. This is clearly seen when considering the signature quantum number in the limit of vanishing rotational frequency Ω_x (see Ref. [77]). In this case definite relations exist between the states $|\nu, r_\nu\rangle$ of good signature r_ν (ν denotes the set of additional quantum numbers) and the single-particle states employed, usually in the low-spin limit. For the latter states in axially symmetric nuclei, we obtain doubly degenerate single-particle states $|\nu, \Omega_\nu\rangle$ and $|\nu, \bar{\Omega}_\nu\rangle$, where Ω_ν denotes the projection of the angular momentum on the symmetry axis. Here, $|\nu, \Omega_\nu\rangle$ is an eigenstate with definite angular momentum projection Ω_ν, whereas $|\nu, \bar{\Omega}_\nu\rangle$ denotes the time-reversed state (with angular momentum projection $-\Omega_\nu$). In the limit of vanishing rotational frequency $\Omega_x = 0$, the states $|\nu, r_\nu\rangle$ with definite signature r_ν become linear combinations of the states $|\nu, \Omega_\nu\rangle$ and $|\nu, \bar{\Omega}_\nu\rangle$:

$$\begin{aligned} |\nu, r_\nu = -i\rangle &= \frac{1}{\sqrt{2}}\{-|\nu, \Omega_\nu\rangle + (-1)^{\Omega_\nu - 1/2}|\nu, \bar{\Omega}_\nu\rangle\}, \\ |\nu, r_\nu = +i\rangle &= \frac{1}{\sqrt{2}}\{(-1)^{\Omega_\nu - 1/2}|\nu, \Omega_\nu\rangle + |\nu, \bar{\Omega}_\nu\rangle\}. \end{aligned} \tag{28}$$

These relations may be considered as a transformation between two representations of the single-particle states: the one with good projection Ω_ν (the $|\nu, \Omega_\nu\rangle$ representation) and the other with good signature r (cranking representation). In the $|\nu, \Omega_\nu\rangle$-representation the alignment of the angular momentum vector of a particle is specified along the axis of symmetry. As a result, the axial symmetry is conserved and only azimuthal currents with respect to the symmetry axis are present. In the cranking formalism (which also allows triaxial shapes), alignment of the angular momentum vector of a particle is specified along the x axis perpendicular to the axis of symmetry. As a result, the

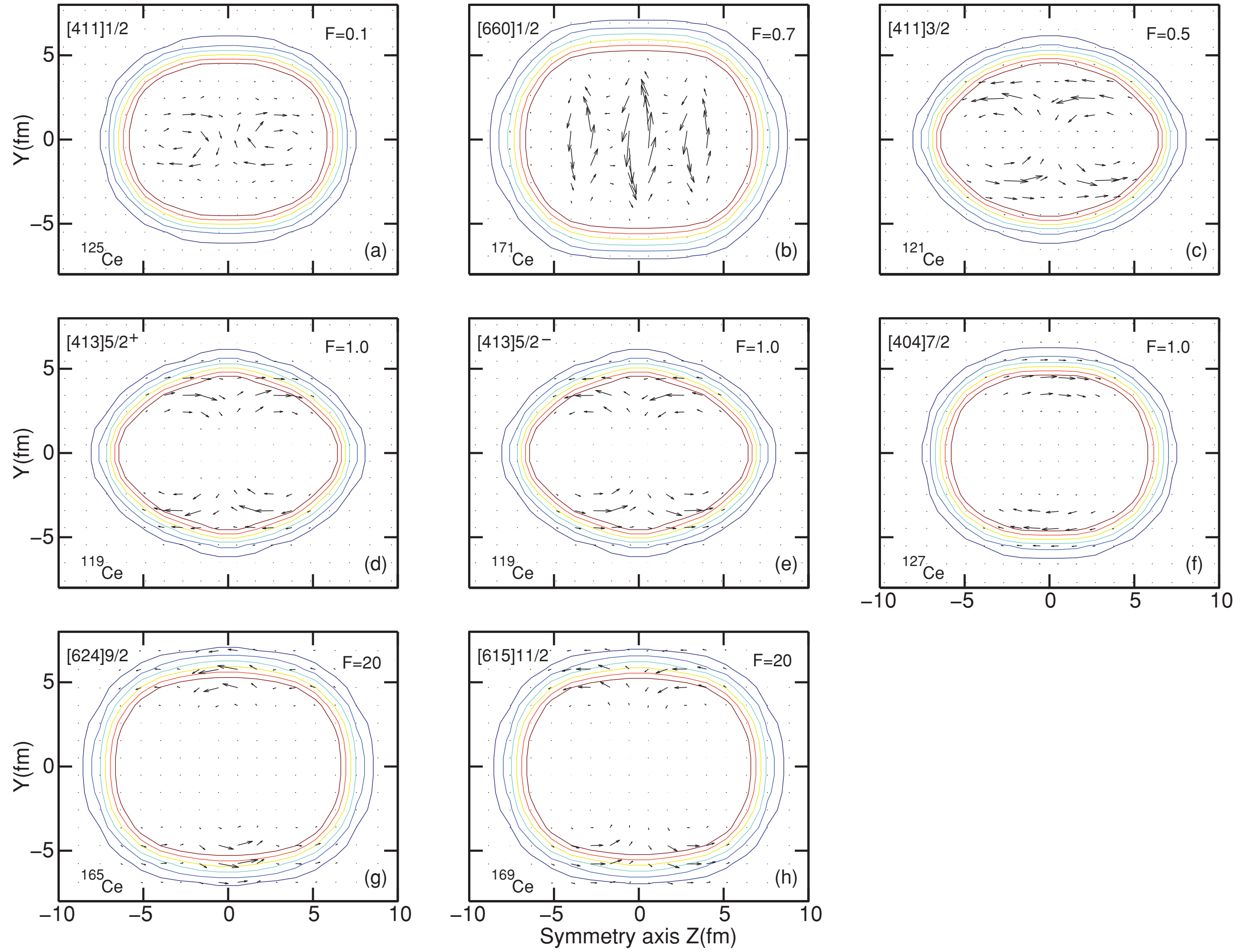

FIG. 6. (Color online) Total neutron current distributions $\boldsymbol{j}^n(\boldsymbol{r})$ in the intrinsic frame in the y–z plane at $x = 0.48$ fm for several configurations with signature ($r = +i$) in Ce nuclei. The only exceptions are the $[413]5/2^{\pm}$ configurations in ^{119}Ce, for which both signatures are shown in (d) and (e). Nilsson quantum numbers $[Nn_z\Lambda]\Omega$ indicate the blocked state. Currents in (d) and (e) are plotted at arbitrary units for better visualization. Currents in other panels are normalized to the currents in (d) and (e) by using factor F. This factor was chosen in such a way that the current distribution for every nucleus is clearly shown. The shape and size of the nucleus are indicated by density lines, which are plotted in the range 0.01–0.06 fm^{-3} in steps of 0.01 fm^{-3}. The panels are arranged so that the Ω value of the Nilsson label of the blocked state increases on going from (a) to (h).

currents follow the symmetries of the cranking approximation and have the distributions discussed here.

Total neutron current distributions in the configurations of selected nuclei having similar quadrupole deformations are shown in Figs. 6 and 7. They are predominantly defined by the currents generated by the blocked orbitals. This is clearly visible from a comparison of Figs. 6 and 8: the latter figure shows the currents produced by a single neutron in different

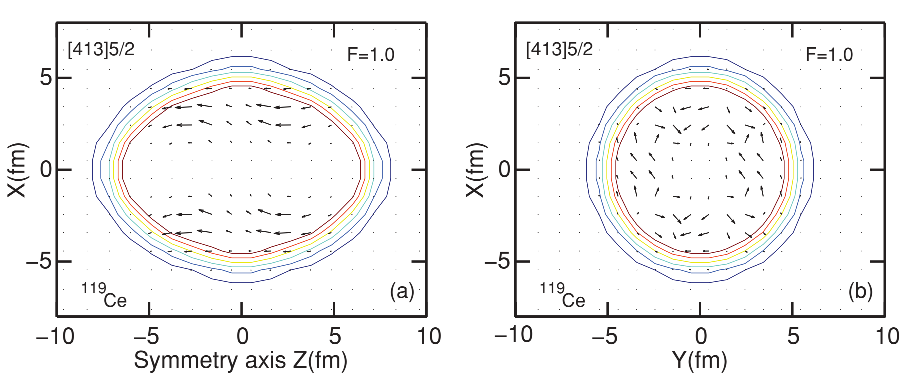

FIG. 7. (Color online) The same as Fig. 6 but for neutron current distributions $\boldsymbol{j}^n(\boldsymbol{r})$ in the z–x plane (at $y = 0.48$ fm) and in the y–x plane (at $z = 0.53$ fm) for the $\nu[413]5/2^+$ configuration of ^{119}Ce.

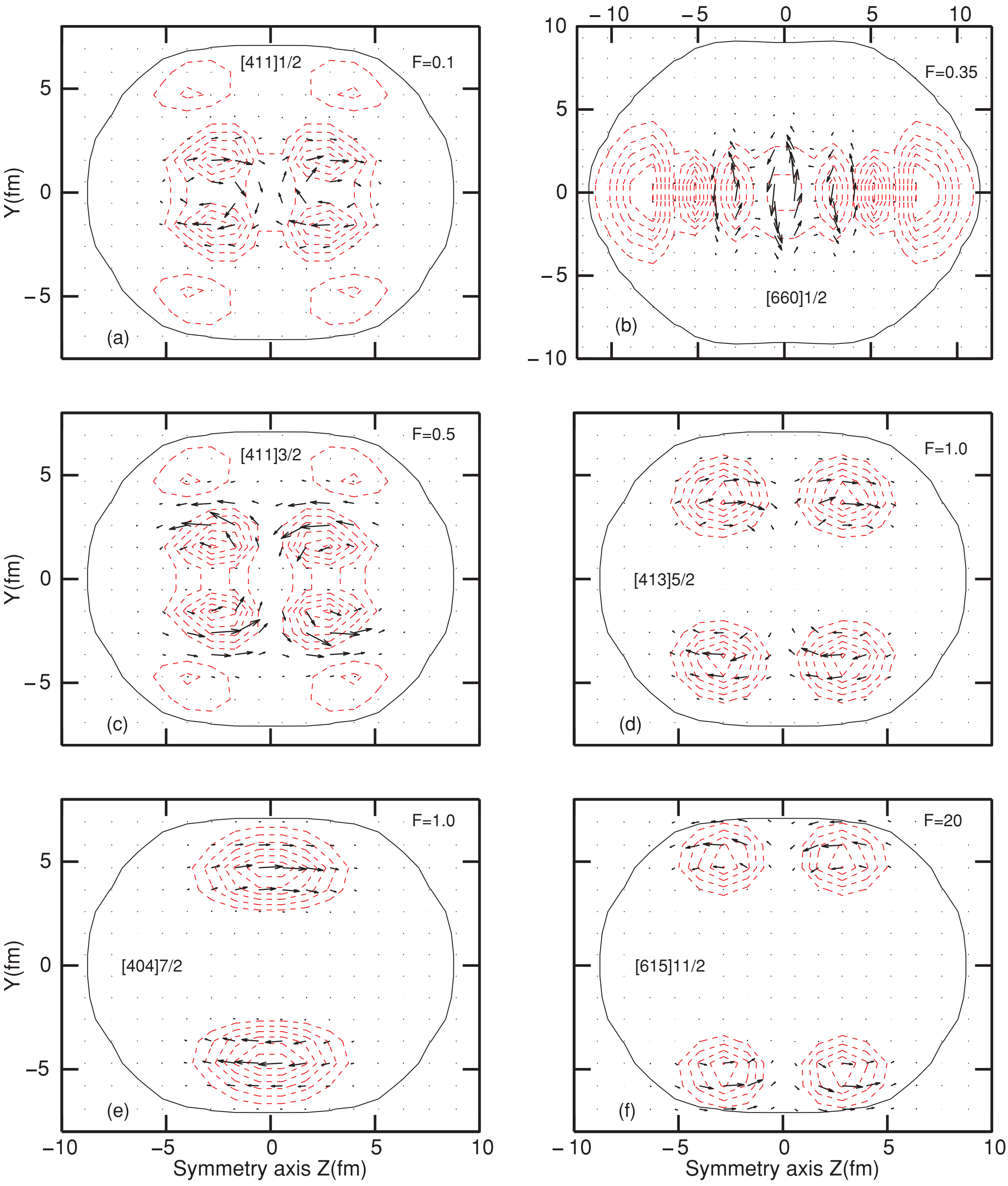

FIG. 8. (Color online) Current distributions $\boldsymbol{j}^n(\boldsymbol{r})$ produced by single neutron in indicated single-particle states with signature ($r = +i$) of the $\nu[660]1/2$ configuration in ^{171}Ce. The shape and size of the nucleus are indicated by the density line, which is plotted at $\rho = 0.01$ fm^{-3} [$\rho = 0.0005$ fm^{-3} in (b)]. The single-neutron density distribution owing to the occupation of the indicated Nilsson state is plotted starting with $\rho = 0.0005$ fm^{-3} in steps of 0.0005 fm^{-3} [0.0003 fm^{-3} in (d)–(f)]. Currents in (d) are plotted at arbitrary units for better visualization. Currents in other panels are normalized to the currents in (d) by using factor F. Currents and densities are shown in the intrinsic frame in the y–z plane at $x = 0.48$ fm.

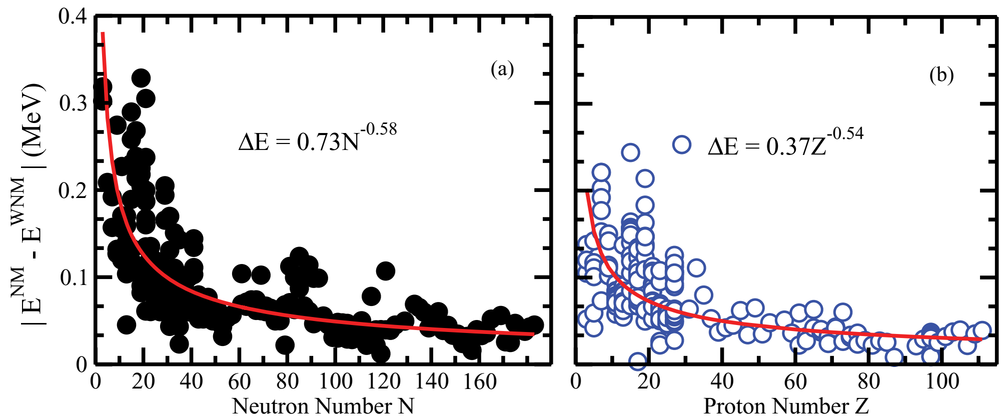

FIG. 9. (Color online) Neutron (a) and proton (b) dependences of additional binding owing to NM. Open and filled circles are used for odd-proton and odd-neutron nuclei, respectively.

Nilsson states of the $\nu[660]1/2$ configuration in ^{171}Ce. Neutron currents are characterized by complicated patterns in different cross sections of the nucleus. Figure 8 clearly shows that these patterns are defined by the density distributions of the blocked states. Moreover, there are clear correlations between the patterns of the currents in the y–z plane (z is the symmetry axis and x is the rotation axis in the CRMF theory) and the Ω value of the Nillson label of the blocked orbital (Figs. 6 and 8). At $\Omega = 1/2$, the single-particle densities are concentrated in the vicinity of the axis of symmetry, and as a consequence, the currents show circulations (vortices) that are concentrated in the central region of the nucleus. However, with increasing Ω, the densities (and, as a consequence, the currents) are pushed away from the axis of symmetry of the nucleus toward the surface area. In addition, the strength of the currents correlates with Ω. As follows from the values of factor F the strongest currents appear for the $\Omega = 1/2$ states. These orbitals are aligned with the axis of rotation (x axis) already at no rotation. As a result, the single-particle angular momentum vector of the $\Omega = 1/2$ orbitals performs the precession around the x axis, thus orienting the currents predominantly in the y–z plane. This extra mechanism is not active in other configurations. The strength of the currents decreases with the increase in Ω. For example, currents generated by the blocked $\Omega = 11/2$ orbitals are weaker by a factor of almost 200 than currents generated by the blocked $\Omega = 1/2$ orbitals (compare scaling factors F in Fig. 6 for blocked states with different Ω values).

In the x–y plane, the majority of the configurations show the current pattern (although with different strengths of the currents and their localization in space) illustrated in Fig. 7(b); the typical pattern of currents in the x–z plane is shown in Fig. 7(a). Figures 6(d) and 6(e) show that the change of the signature of the blocked orbital leads only to a change in the direction of the currents.

D. Particle number dependences of additional binding owing to nuclear magnetism

Neutron and proton number dependences of additional binding owing to NM (the $|E^{\rm NM} - E^{\rm WNM}|$ quantity) are presented in Fig. 9. These figures are based on the results obtained in Sec. III A and Sec. III B and on some extra calculations. These extra calculations include odd-Z nuclei with $N = 94$, odd-N nuclei with $Z = 98$, and odd-Z nuclei with $N = 154$ and cover these isotope and isotone chains from proton to neutron drip lines.

Calculations of nuclei around ^{249}Cf were also performed to check the impact of pairing on the $(E^{\rm NM} - E^{\rm WNM})$ quantity. For the same blocked states, the $(E^{\rm NM} - E^{\rm WNM})$ values obtained in the calculations without pairing in the present article were compared with those obtained in the relativistic Hartree-Bogoliubov calculations in Ref. [32] (see Table IV in Ref. [32]). Although the pairing decreases additional binding owing to NM in most cases, there are still one (quasi)-particle configurations in which the $|E^{\rm NM} - E^{\rm WNM}|$ quantity is smaller in the calculations without pairing. This is a consequence of the complicated nature of the $E^{\rm NM} - E^{\rm WNM}$ quantity defined by (i) the interplay of time-odd mean fields and the polarization effects (Sec. IV) and (ii) the differences in the impact of pairing on different terms of the total energy.

The calculated $|E^{\rm NM} - E^{\rm WNM}|$ quantities were fitted by simple parametrization,

$$\Delta E = \frac{c}{Q^{\alpha}}, \tag{29}$$

where Q is equal to either proton Z or neutron N numbers. Note that the $|E^{\rm NM} - E^{\rm WNM}|$ values from odd-proton (odd-neutron) nuclei were used in the fit of Z (N) dependence of ΔE. The results of the fits are shown by solid lines in Fig. 9. One can see that the powers α are similar for different fits (proton or neutron). On the other hand, the magnitudes c differ considerably between proton and neutron quantities, indicating weaker additional binding owing to NM for odd-proton nuclei. This result is consistent with the analysis in Sec. VI.

The three-point indicator [66],

$$\Delta^{(3)}(N) = \frac{\pi_N}{2}[B(N-1) + B(N+1) - 2B(N)], \tag{30}$$

is frequently used to quantify the odd-even staggering (OES) of binding energies. Here $\pi_N = (-1)^N$ is the number parity and $B(N)$ is the (negative) binding energy of a system with N

particles. In Eq. (30), the number of protons Z is fixed, and N denotes the number of neutrons, that is, this indicator gives the neutron OES. The factor depending on the number parity π_N is chosen so that the OESs centered on even and odd neutron number N will both be positive. An analogous proton OES indicator, $\Delta^{(3)}(Z)$, is obtained by fixing the neutron number N and replacing N with Z in Eq. (30).

The $\Delta^{(3)}(N)$ [and, similarly, the $\Delta^{(3)}(Z)$] quantity will be modified in the presence of time-odd mean fields as

$$\Delta^{(3)}_{\mathrm{TO}}(N) = \Delta^{(3)}_{\mathrm{WTO}}(N) + \delta E_{\mathrm{TO}}, \tag{31}$$

where the subscripts TO and WTO indicate the values obtained in calculations with and without time-odd mean fields, and δE_{TO} is the contribution coming from time-odd mean fields. If the $\Delta^{(3)}(N)$ quantity is centered at an odd-N nucleus, the δE_{TO} quantity represents the change in binging energy of this odd-mass nucleus induced by time-odd mean fields. This is because the time-odd mean fields have no effect on the binding energies of the ground states of even-even nuclei. Note that with such selection δE_{TO} is negative if the time-odd mean fields provide additional binding in the odd-mass nucleus.

In the CDF theory, the δE_{TO} quantity is equal to $E^{\mathrm{NM}} - E^{\mathrm{WNM}}$ and thus it is always negative: This result does not depend on the RMF parametrization (see Sec. III A for the dependence of the $E^{\mathrm{NM}} - E^{\mathrm{WNM}}$ quantity on the RMF parametrization). In addition, the magnitude of the δE_{TO} quantity depends only weakly on the RMF parametrization. On the contrary, the sign and the magnitude of δE_{TO} depends strongly on the parametrization in the Skyrme EDF calculations. For example, in calculations with the SLy4 force the δE_{TO} quantity is positive for medium-mass nuclei [31,67,68] but negative in light nuclei [30]. On the other hand, the δE_{TO} quantity will be positive in light nuclei in calculations with the SIII parametrizations [30].

It is interesting to compare the averaged effects of time-odd mean fields as given by the ΔE quantity with the experimental global trends for OES as shown by dashed lines in Fig. 2 in Ref. [67]. The latter trends were obtained using phenomenological parametrization with the same functional dependence as in Eq. (29) with $c = 4.66$ MeV (4.31 MeV) and $\alpha = 0.31$ for neutron (proton) data sets. Comparison of theory and experiment suggests that time-odd mean-field contributions to OES can be as large as 10% in light systems and about 5%–6% in heavy systems. These are non-negligible contributions that have to be taken into account when the strength of the pairing interaction is defined from the fits to experimental OES. The analysis of Sn isotopes in Ref. [35] showed that time-even and time-odd polarization effects induced by odd nucleons produce OES reduced by about 30% compared to that obtained in standard spherical calculations. As a consequence, an enhancement of pairing strength by about 20% is required to compensate for that effect. Our calculations show a much smaller reduction of OES, in part because the polarization effects in the time-even channel are already taken into account in the calculations without NM. Thus, the current calculations suggest that a much smaller increase in the strength of pairing (by approximately 5%) would be required to compensate for the reduction in OES owing to time-odd mean fields.

IV. THE MECHANISM OF ADDITIONAL BINDING OWING TO NUCLEAR MAGNETISM IN ODD-MASS NUCLEI

In this section, a detailed analysis of the impact of NM on the energies of single-particle states and on different terms in the total energy expression [Eq. (15)] is performed to better understand the microscopic mechanism of additional binding owing to NM. We use the $\nu[413]5/2$ configuration of ^{119}Ce as an example in this analysis.

A. Energy splittings of time-reversal counterpart single-particle states in the presence of nuclear magnetism

Figure 10 shows that the presence of time-odd mean fields leads to the energy splitting $\Delta E_{\mathrm{split}}(i)$ of the single-particle states that are time-reversal counterparts. This corresponds to the removal of the Kramer's degeneracy of these states. One of these states moves up by $\approx\Delta E_{\mathrm{split}}/2$ compared with its position in the absence of NM, whereas another moves down by $\approx\Delta E_{\mathrm{split}}/2$.

Detailed analysis of the single-particle spectra in ^{119}Ce and ^{123}Xe reveals general features that are also found in other nuclei. The ^{119}Ce nucleus is axially symmetric ($\gamma = 0^\circ$), whereas ^{123}Xe is triaxial with $\gamma = -26^\circ$. This difference in the symmetry of the nucleus results in important consequences: the energy splittings appear in all single-particle states in triaxial nuclei, whereas only states with $\Omega = \Omega_{\mathrm{bl}}$ (the subscript

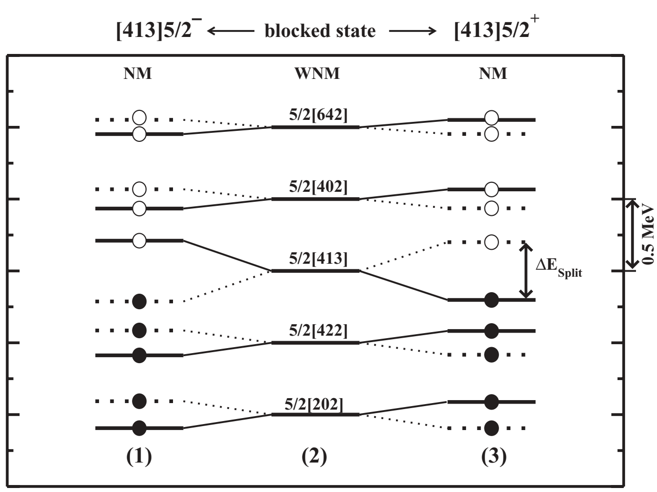

FIG. 10. Columns (1) and (3): energy splittings $\Delta E_{\mathrm{split}}$ between different signatures of single-particle states in the presence of NM. Results of the calculations are shown for configurations of ^{119}Ce in which either the $\nu[413]5/2^-$ [column (1)] or the $\nu[413]5/2^+$ [column (3)] states are blocked. These signatures are degenerated in energy in calculations without NM [column (2)]. Note that the single-particle states of interest are shown at arbitrary absolute energy in column (2). Filled and open circles indicate occupied and unoccupied states, respectively. Solid and dotted lines are used for the $r = +i$ and $(r = -i)$ states, respectively.

"bl" indicates the blocked state) experience such splittings in axially symmetric nuclei. The former feature is because Ω is not a good quantum number in triaxial nuclei and each single-particle state represents a mixture of the basic states with different values of Ω.

It is important to mention that occupied and unoccupied states as well as proton and neutron states show energy splittings (Fig. 10). Splittings of the proton and neutron states of the same structure are similar. This is because the largest contribution to the magnetic potential [Eq. (5)] is due to space-like components of the ω-meson fields that do not depend on the isospin. In addition, the occupied state is always more bound than its unoccupied time-reversal counterpart.

A change in the signature of the blocked state leads to an inversion of the signatures in all pairs of time-reversal orbitals [compare columns (1) and (3) in Fig. 10]. The explanation of this process is as follows. The change in the signature of the blocked state results in a change in the direction of the currents to the opposite one [compare Figs. 6(d) and 6(e)]. This leads to a change in the direction of the vector potential $\boldsymbol{V}(\boldsymbol{r})$ in the Dirac equation to the opposite one, which in turn causes inversion of the signatures in all pairs of time-reversal orbitals. However, the additional binding owing to NM (the $E^{\rm NM} - E^{\rm WNM}$ quantity) does not depend on the signature of the blocked state in odd-mass nuclei.

B. Polarization effects induced by nuclear magnetism

The polarization effects induced by NM were investigated by considering its impact on different terms of the total energy [Eq. (15)]. The results of this study are reported in Table I. One can see that the total energy terms can be split into two groups, dependent on how they are affected by NM. The first group includes the $E_{\sigma{\rm NL}}$, $E_{\rho}^{\rm TL}$, $E_{\rho}^{\rm SL}$ and $E_{\rm Coul}$ terms, which are only weekly influenced by NM, and thus, they are not discussed in detail.

The second group is represented by the $E_{\rm part}$, E_σ, $E_\omega^{\rm TL}$, and $E_\omega^{\rm SL}$ terms, which are strongly affected by NM. The $E_\omega^{\rm SL}$ term is directly connected with the nucleonic currents [see Eq. (21)]. The E_σ and $E_\omega^{\rm TL}$ terms depend only indirectly on time-odd mean fields: the minimization of the total energy in the presence of time-odd terms leads to a very small change in equilibrium deformation induced by NM. The quadrupole and hexadecapole moments change by 10^{-4} of their absolute value when the NM is switched on; a similar magnitude of changes is seen also in E_σ and $E_\omega^{\rm TL}$. One should keep in mind that only the $E_\sigma + E_\omega^{\rm TL}$ quantity has a deep physical meaning, as it defines a nucleonic potential; this sum is modified by NM only at -177 keV.

The largest modification (by -410 keV) is seen in the $E_{\rm part}$ energy, with half of it coming from the change in the single-particle energy (by ≈ -200 keV) of the blocked orbital (the $\nu[413]5/2$ orbital) in the presence of NM. Note that because both signatures of other pairs of time-reversal orbitals below the Fermi level are occupied, the large energy splittings $E_{\rm split}$ seen for some of them do not have a considerable impact on $E_{\rm part}$ [see Eq. (16)], as this splitting is nearly symmetric with respect to the position of these orbitals in the absence of NM. Thus, the rest of the modification of $E_{\rm part}$ is related to small changes in the single-particle energies of occupied states caused by the changes in the equilibrium deformation induced by NM.

This detailed analysis clearly indicates that the $E^{\rm NM} - E^{\rm WNM}$ quantity is defined by both time-odd mean fields and the polarization effects in time-even mean fields induced by time-odd mean fields. $E^{\rm NM} - E^{\rm WNM} = -104$ keV is a result of near-cancellation of the contributions owing to fermionic (-410 keV) and mesonic (-306 keV) degrees of freedom. Note that the latter appears with a negative sign in Eq. (15). The fermionic degrees of freedom are represented by the $E_{\rm part}$ and $E_{\rm cm}$ terms, whereas the other terms of the total energy are related to the mesonic degrees of freedom. The fermionic contribution to $E^{\rm NM} - E^{\rm WNM}$ is defined by more or less equal contributions from time-odd mean fields and the polarization effects in time-even fields. On the contrary, time-odd mean fields define only approximately one-third ($E_\omega^{\rm SL} = -0.124$ keV) of the mesonic contribution to $E^{\rm NM} - E^{\rm WNM}$, whereas the rest is caused by polarization effects in time-even mean fields.

It turns out that these contributions are highly correlated, as can be seen from the ratio $\Delta E_{\rm split}/(E^{\rm NM} - E^{\rm WNM})$ in the Ce isotope chain (Fig. 11). $\Delta E_{\rm split}$ depends only on time-odd mean fields in the fermionic channel, whereas $(E^{\rm NM} - E^{\rm WNM})$ depends both on time-odd mean fields and on the polarizations effects in time-even mean fields in fermionic and mesonic channels. One can see that $\Delta E_{\rm split}/(E^{\rm NM} - E^{\rm WNM}) \approx 4$ for the majority of nuclei. A similar relation also exists in the Skyrme EDF calculations for Ce isotopes (see Eq. (7) in Ref. [31]).

The impact of NM on different terms of the total energy in the $\nu[606]13/2^+$ configuration of the ^{183}Ce nucleus, which is located at the neutron drip line, is reported in Table II. A comparison of Tables I and II clarifies the microscopic origin of the general trend, which shows the decrease in the impact of

TABLE I. Impact of NM on different terms of the total energy [Eq. (15)] in the $[413]5/2^+$ configuration of ^{119}Ce. Column (2) lists the absolute energies (MeV) of different energy terms in the case where NM is neglected. Columns (3) and (4) list the changes $\Delta E_i = E_i^{\rm NM} - E_i^{\rm WNM}$ (MeV) in the energies of these terms induced by NM in self-consistent [column (3)] and perturbative [column (4)] calculations. Note that only nonzero quantities are listed in column (4). Relevant quantities are also listed for the kinetic energy $E_{\rm kin}$ [Eq. (26)] in the last row.

Quantity (1)	$E_i^{\rm WNM}$ (2)	ΔE_i (3)	$\Delta E_i^{\rm pert}$ (4)
$E_{\rm part}$	-2849.889	-0.410	-0.237
E_σ	-17079.532	-2.231	
$E_{\sigma{\rm NL}}$	343.341	-0.017	
$E_\omega^{\rm TL}$	14356.156	2.054	
$E_\omega^{\rm SL}$	0.0	-0.124	-0.124
$E_\rho^{\rm TL}$	2.044	0.003	
$E_\rho^{\rm SL}$	0.0	-0.010	-0.010
$E_{\rm Coul}$	481.196	0.017	
$E_{\rm cm}$	-6.252	0.0	
$E_{\rm tot}$	-959.349	-0.104	-0.103
$E_{\rm kin}$	1630.386	-0.099	-0.237

TABLE II. The same as Table I but for the [606]13/2$^+$ configuration of ^{183}Ce.

Quantity (1)	$E_i^{\rm WNM}$ (2)	ΔE_i (3)	$\Delta E_i^{\rm pert}$ (4)
$E_{\rm part}$	−4139.512	−0.157	−0.095
E_σ	−23720.872	−0.608	
$E_{\sigma\rm NL}$	541.423	−0.004	
$E_\omega^{\rm TL}$	19696.151	0.538	
$E_\omega^{\rm SL}$	0.0	−0.043	−0.043
$E_\rho^{\rm TL}$	236.863	0.009	
$E_\rho^{\rm SL}$	0.0	−0.005	−0.005
$E_{\rm Coul}$	437.326	0.002	
$E_{\rm cm}$	−5.416	0.0	
$E_{\rm tot}$	−1335.818	−0.045	−0.047
$E_{\rm kin}$	2561.558	−0.045	−0.095

NM [reflected in the ($E^{\rm NM} - E^{\rm WNM}$) quantity] with increasing particle (proton, neutron, or mass) number (see Figs. 2 and 9). In the ^{183}Ce nucleus, the impact of NM on the $E_\omega^{\rm SL}$ and $E_\rho^{\rm SL}$ terms, which directly depend on time-odd mean fields, decreases by factors of close to 3 and 2 relative to the ^{119}Ce case (see Table I), respectively. The impact of NM on the E_σ, $E_{\sigma\rm NL}$, $E_\omega^{\rm TL}$, $E_\rho^{\rm TL}$, $E_{\rm Coul}$ terms, which depend on time-odd mean fields only through polarization effects, decreases even more dramatically (by a factor of close to 4). Note that the contribution of the ρ meson to the ($E^{\rm NM} - E^{\rm WNM}$) quantity is marginal even at the neutron drip line. Other investigated cases also indicate a decrease in the impact of NM with increasing particle number.

The general trend of a decrease in the impact of NM on binding energies with increasing particle number can be understood in the following way. The effects attributable to NM are produced by an odd particle that breaks time-reversal symmetry. With increasing particle (proton, neutron, or mass) number the nucleus becomes larger and thus more robust to

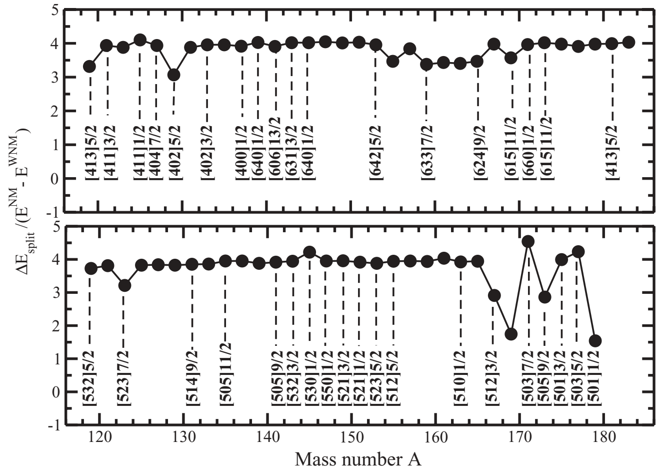

FIG. 11. The ratio $\Delta E_{\rm split}/(E^{\rm NM} - E^{\rm WNM})$ in Ce isotopes. The structure of blocked states is shown by the Nilsson labels; the states at and to the right of the Nilsson label up to the next Nilsson label have the same blocked state.

time-odd and polarization effects induced by the odd particle (or, in other words, the effective impact of the single particle on the total nuclear properties becomes smaller).

It is interesting to compare the results of self-consistent and perturbative calculations. The $\Delta E_i = E_i^{\rm NM} - E_i^{\rm WNM}$ quantities are used for simplicity in further discussion. These quantities are listed in columns (3) and (4) in Tables I and II. The ΔE_σ, $\Delta E_{\sigma\rm NL}$, $\Delta E_\omega^{\rm TL}$, and $\Delta E_\rho^{\rm TL}$ quantities are zero in perturbative calculations. $\Delta E_{\rm Coul} = 0$ for odd-neutron systems in perturbative calculations (Tables I and II), but it can differ from zero in systems containing an odd number of protons (Tables III and IV). The results of self-consistent and perburbative calculations for the $\Delta E_\omega^{\rm SL}$ and $\Delta E_\rho^{\rm SL}$ quantities are the same with the exception of configuration B in ^{34}Cl, where only a small difference exists (Tables I, II, and IV).

It is evident from Tables I and II that

$$\Delta E_{\rm tot}^{\rm self\text{-}const} \approx \Delta E_{\rm tot}^{\rm pert} \tag{32}$$

for odd-neutron nuclei. Note that the superscript "self-const" refers to fully self-consistent results. Figure 12 shows that this equality is fulfilled in the majority of nuclei of the Fe and Ce isotope chains with a high degree of accuracy (compared with the $E^{\rm NM} - E^{\rm WNM}$ quantities). *These results clearly indicate that the additional binding owing to NM (the $E^{\rm NM} - E^{\rm WNM}$ quantity) is defined mainly by time-odd fields and that the polarization effects in fermionic and mesonic sectors of the model cancel each other to a large degree.*

As a consequence it is important to understand the relations between different polarization effects. The particle energy $E_{\rm part}^{\rm self\text{-}const}$ obtained in self-consistent calculations can be split into two parts: the part $E_{\rm part}^{\rm TO}$, which directly depends on time-odd mean fields, and the part $E_{\rm part}^{\rm pol}$, which is defined by the polarization effects in the fermionic sector of the model. Thus, $E_{\rm part}^{\rm self\text{-}const} = E_{\rm part}^{\rm TO} + E_{\rm part}^{\rm pol}$ and $E_{\rm part}^{\rm pert} \approx E_{\rm part}^{\rm TO}$. Taking into account Eq. (15) and the afore-mentioned features of the $\Delta E_i^{\rm pert}$ terms, one can conclude that

$$\Delta E_{\rm part}^{\rm pol} = \Delta E_\sigma^{\rm self\text{-}const} + \Delta E_{\sigma\rm NL}^{\rm self\text{-}const} + \Delta E_\omega^{\rm TL[self\text{-}const]} + \Delta E_\rho^{\rm TL[self\text{-}const]} + \Delta E_{\rm Coul}^{\rm self\text{-}const}. \tag{33}$$

This relation clearly indicates that the polarization effects in the fermionic ($E_{\rm part}^{\rm pol}$ term) and mesonic ($\Delta E_\sigma^{\rm self\text{-}const}$, $\Delta E_{\sigma\rm NL}^{\rm self\text{-}const}$, $\Delta E_\omega^{\rm TL[self\text{-}const]}$, and $\Delta E_\rho^{\rm TL[self\text{-}const]}$ terms) sectors of the model are strongly correlated. Equation (33) also clarifies the physical origin of $\Delta E_{\rm part}^{\rm pol}$. The terms on the right-hand side are related to the change in the nucleonic potential induced by NM. This change leads to modifications of the single-particle energies of all occupied states (compared with the case when NM is absent), which are reflected in $\Delta E_{\rm part}^{\rm pol}$. On the contrary, the $\Delta E_{\rm part}^{\rm TO}$ is caused by the breaking of the Kramer's degeneracy between the blocked state and its unoccupied time-reversal counterpart. Note that $\Delta E_{\rm part}^{\rm TO} \approx -\frac{1}{2}\Delta E_{\rm split}$ (the minus sign reflects the fact that the blocked state is always more bound in the presence of NM) and the $\Delta E_{\rm split}$ values obtained in self-consistent and perturbative calculations are the same for the pairs of time-reversal counterpart states involving the blocked state.

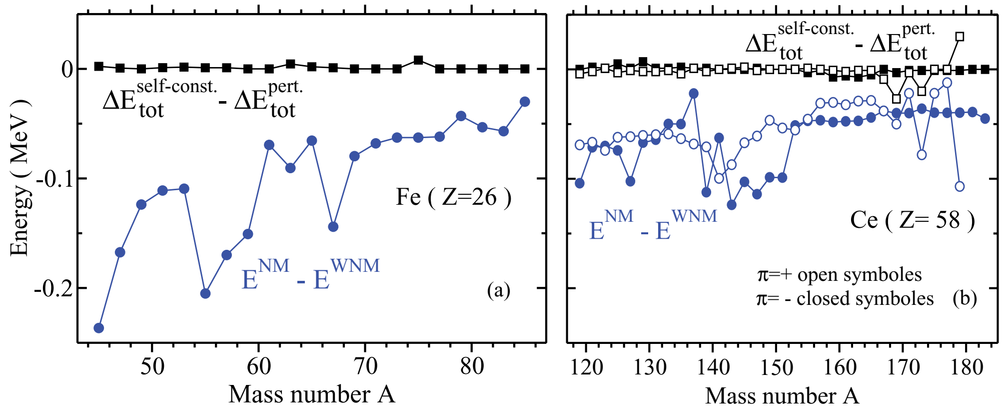

FIG. 12. (Color online) The $\Delta E_{\rm tot}^{\rm self\text{-}const} - \Delta E_{\rm tot}^{\rm pert}$ and $E^{\rm NM} - E^{\rm WNM}$ quantities for odd-neutron Fe and Ce nuclei.

A relation similar to Eq. (32) also exists in odd-proton nuclei, but in this case it has to be corrected for the $\Delta E_{\rm Coul}^{\rm pert}$ energy change:

$$\Delta E_{\rm tot}^{\rm self\text{-}const} \approx \Delta E_{\rm tot}^{\rm pert} + E_{\rm Coul}^{\rm pert}. \tag{34}$$

Figure 13 shows that this relation is fulfilled in odd-proton $N = 94$ nuclei with a high degree of accuracy (compared with the $E^{\rm NM} - E^{\rm WNM}$ quantities). Equation (34) also leads to the condition of Eq. (33) and to the interpretation of $E_{\rm part}^{\rm pol}$ discussed previously.

V. THE IMPACT OF TIME-ODD MEAN FIELDS ON THE PROPERTIES OF PROTON-UNSTABLE NUCLEI

The blocked state always has a lower energy than its unoccupied time-reversal counterpart in calculations with NM; this fact does not depend on the signature of the blocked state (Sec. IV A). The energy of the blocked state in the presence of NM is lower by $\approx \Delta E_{\rm split}/2$ than the energy of the same state in the absence of NM. This additional binding will affect the properties of the nuclei in the vicinity of the proton drip line via two mechanisms, discussed here. They are illustrated schematically in Fig. 14.

In the first mechanism, the nucleus, which is proton unbound (state A in Fig. 14) in calculations without NM, becomes proton bound in calculations with NM (state A' in Fig. 14). The necessary condition for this mechanism to be active is the requirement that the energy of the single-particle state in the absence of NM is less than $\Delta E_{\rm split}/2$. This mechanism can be active in both the ground and the excited states of the nuclei in the vicinity of the proton drip line.

In the second mechanism, the energy of the single-particle state (state B' in Fig. 14) is lower in the presence of NM, but the state still remains unbound. This will affect the decay properties of proton emitters and the possibilities of their observation. Indeed, the lowering of the energy of the single-proton state will decrease the probability of emission of the proton through a combined Coulomb and centrifugal barrier. Many results on the physics of proton emitters are conventionally expressed in terms of the Q_p energies, which depend on the difference in the binding energies of parent (odd-proton) and daughter (even-proton) nuclei. Note that for simplicity we consider here only even-N nuclei. NM leads to an additional binding in an odd-proton nucleus but it does not affect the binding of an even-proton nucleus. Thus, the Q_p

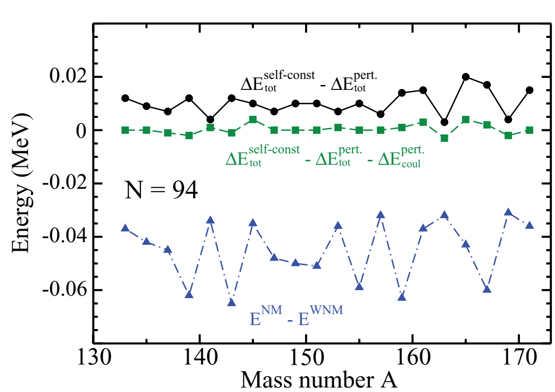

FIG. 13. (Color online) The same as Fig. 12, but for odd-proton $N = 94$ nuclei.

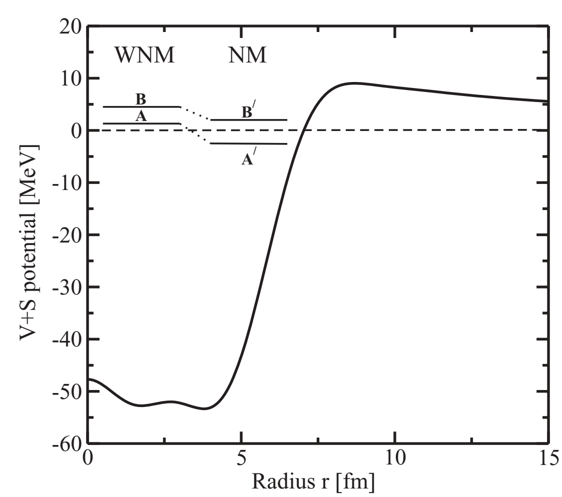

FIG. 14. Schematic illustration of the impact of time-odd mean fields on the properties of odd-proton nuclei in the vicinity of the proton drip line. The single-proton states, involved in the mechanisms discussed in the text, and proton nucleonic potential (which also includes the Coulomb potential) are shown.

values are lower by the value of this additional binding when the NM is taken into account.

Two consequences follow from lower Q_p values. First, experimental observation of proton emission from the nucleus becomes impossible if the Q_p value moves outside the Q_p window favorable for the observation of proton emission or becomes possible if the Q_p value moves into the Q_p window favorable for the observation of proton emission. The size of the Q_p window for rare-earth proton emitters is about 0.8–1.7 MeV, whereas it is much smaller in lighter nuclei [69,70]. Large Q_p values outside this window result in extremely short proton-emission half-lives, which are difficult to observe experimentally. On the other hand, the decay width is dominated by β^+ decay for low Q_p values, below the Q_p window. This consequence of the lowering of Q_p owing to NM is especially important in light nuclei, where the impact of NM on binding energies is especially pronounced and the Q_p window is narrow.

Second, the lowering of the Q_p values owing to NM will increase the half-lives of proton emitters. For example, the lowering of Q_p owing to NM will be around 50 keV in the rare-earth region, as this is a typical value for additional binding owing to NM in odd-mass nuclei in this region (Sec. III B). This can increase the half-lives of proton emitters by a factor of ≈ 2 at the upper end of the Q_p window and by a factor of ≈ 4 at the lower end of the Q_p window (see Fig. 5 in Ref. [70]). The effects of NM have been neglected in the existing RHB studies of proton emitters with $Z \geqslant 50$ (see, e.g., Ref. [71]) but this should not introduce significant error in this mass region.

On the other hand, the impact of NM on the half-lives of proton emitters in lighter nuclei can be dramatic. This is attributable to two factors, namely, (i) the general increase in additional binding owing to NM and the magnitude of the $\Delta E_{\mathrm{split}}$ with decreasing mass and (ii) the narrowing of the Q_p window with the decrease in mass caused by the lowering of the Coulomb barrier. This can be illustrated by several examples. The change in proton energy of around 300 keV in ^{69}Br causes a change in the proton decay lifetime of 11 orders of magnitude [69]. This effect is even more pronounced in lighter systems. The half-life window of 10 to 10^{-4} s corresponds to proton energies of 100–150 keV in nuclei around $Z = 20$ [72], whereas the variation of the Q_p value between 3 and 50 keV in ^{7}B changes the half-lives by 30 orders of magnitude [70]. The energy changes quoted in these examples are either of a similar magnitude as or even smaller than the changes in the energies of single-proton states and the Q_p values induced by NM. As a result, one can conclude that the effects of time-odd mean fields have to be taken into account when attempting to describe the properties of proton emitters in light nuclei.

VI. ODD-ODD MASS NUCLEI: A MODEL STUDY OF THE IMPACT OF NUCLEAR MAGNETISM ON BINDING ENERGIES

The nuclei around ^{32}S in superdeformed minima are considered in the present section. Their selection is guided in part by the desire to compare the CRMF results with those obtained in the Skyrme EDF in Ref. [73], where the signature

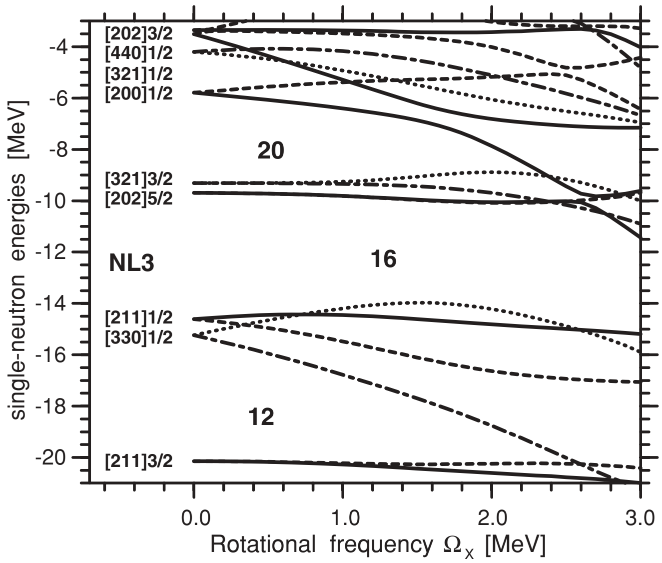

FIG. 15. Neutron single-particle energies (Routhians) as a function of the rotational frequency Ω_x. They are given along the deformation path of the doubly magic SD configuration $\pi 3^2 \nu 3^2$ in ^{32}S. Solid, short-dashed, dot-dashed, and dotted lines indicate $(\pi = +, r = -i)$, $(\pi = +, r = +i)$, $(\pi = -, r = +i)$, and $(\pi = -, r = -i)$ orbitals, respectively. At $\Omega_x = 0.0$ MeV, single-particle orbitals are labeled by means of the asymptotic quantum numbers $[Nn_z\Lambda]\Omega$ (Nilsson quantum numbers) of the dominant component of the wave function.

separation induced by time-odd mean fields has been found in the excited SD bands of ^{32}S. The CRMF calculations have been performed for some SD configurations in ^{32}S and in neighboring nuclei. The starting point is the doubly magic SD configuration $\pi 3^2 \nu 3^2$ in ^{32}S (hereafter, SD core) (see Ref. [64]), in which all single-particle orbitals below the $N = Z = 16$ SD shell gaps are occupied (Fig. 15). Here the configurations are labeled by the numbers of occupied proton (p) and neutron (n) high-N intruder orbitals (the $N = 3$ orbitals in our case): this is commonly accepted shorthand notation $\pi N^n \nu N^p$ of the configurations in high-spin physics [38]. Then the configurations in the nuclei under consideration (Fig. 16) are created by either adding particles into the [202]$5/2^{\pm}$ orbital(s) and/or creating holes in the [330]$1/2^{\pm}$ orbitals: these are the orbitals active in signature-separated configurations discussed in Ref. [73].

Similar to the results shown in Sec. III A and Sec. III B, NM leads to additional binding in the configurations of odd mass nuclei (the configurations in ^{33}S and ^{33}Cl created by adding a particle to the SD core or the configurations in ^{31}P and ^{31}S created by removing a particle from the SD core; see Fig. 16). This additional binding does not depend on the signature of the blocked state.

Figure 16 shows that additional binding owing to NM is smaller for the configurations with a blocked proton state compared with those with a blocked neutron state. For example, the configurations in ^{31}P and ^{31}S are built on the same blocked Nilsson state. However, additional binding owing to NM is smaller in the odd-proton nucleus (^{31}P) than in the odd-neutron one (^{31}S). A similar situation also exists in ^{33}S and

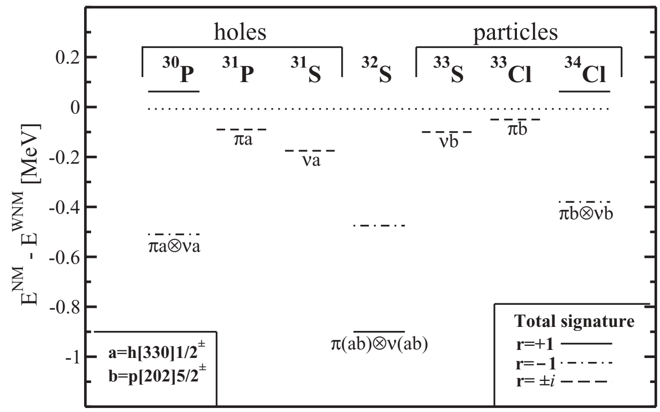

FIG. 16. Impact of NM on binding energies of different configurations under study. Energies of configurations calculated without NM are normalized to zero. To guide the eye the dotted line is used for the zero value of the $E^{\rm NM} - E^{\rm WNM}$ quantity. Short lines show the magnitude of additional gain (negative $E^{\rm NM} - E^{\rm WNM}$ values) or loss (positive $E^{\rm NM} - E^{\rm WNM}$ values) in binding energies in the presence of NM. Short-dashed, solid, and long-dashed lines are used for total signatures $r = -1$, $r = +1$, and $r = \pm i$ of the configuration, respectively. Configurations are labeled by the particle (p) and/or hole (h) states with respect to the ^{32}S SD core: configurations with holes (particles) are shown to the left (right) of ^{32}S.

^{33}Cl. These results are consistent with a general systematics (Sec. III D) showing that additional binding owing to NM is smaller in the proton subsystem than in the neutron one.

The results of perturbative calculations for the configuration with the proton hole in $\pi[330]1/2^-$ in the odd-proton ^{31}P nucleus and for the configuration with the neutron hole in $\nu[330]1/2^-$ in the odd-neutron ^{31}S nucleus are reported in Table III. These hole configurations are formed by removing either a proton (^{31}P) or a neutron (^{31}S) from the $N = Z$ ^{32}S SD core. One can see that the decrease in additional binding owing to NM on going from a neutron to a proton configuration of the same structure can be traced to the changes in the particle energy $\Delta E^{\rm pert}_{\rm part}$, from -0.349 MeV in the odd-neutron ^{31}S nucleus to -0.250 MeV in the odd-proton ^{31}P. This explains the major part of the change in the $\Delta E^{\rm pert}_{\rm tot}$ quantity on going from the odd-neutron ^{31}S ($\Delta E^{\rm pert}_{\rm tot} = -0.165$ MeV) to the odd-proton ^{31}P ($\Delta E^{\rm pert}_{\rm tot} = -0.100$ MeV). The contributions of other terms to $\Delta E^{\rm pert}_{\rm tot}$ on going from the odd-neutron ^{31}S to the odd-proton ^{31}P nucleus are smaller: 0.020, 0.001, and 0.013 MeV for the $\Delta E^{\rm SL}_{\omega}$, $\Delta E^{\rm SL}_{\rho}$, and $\Delta E_{\rm Coul}$ terms, respectively.

TABLE III. The $\Delta E^{\rm pert}_i = (E^{\rm NM}_i - E^{\rm WNM}_i)^{\rm pert}$ quantities for different terms of the total energy [Eq. (15)] for configurations discussed in the text. Only terms affected by NM in perturbative calculations are listed here.

Quantity (1)	^{31}S (2)	^{31}P (3)	^{33}S (4)	^{33}Cl (5)
$\Delta E^{\rm pert}_{\rm part}$	−0.349	−0.250	−0.198	−0.136
$\Delta E^{\rm SL[pert]}_{\omega}$	−0.168	−0.148	−0.093	−0.080
$\Delta E^{\rm SL[pert]}_{\rho}$	−0.016	−0.015	−0.010	−0.009
$\Delta E^{\rm pert}_{\rm Coul}$	0.0	0.013	0	0.010
$\Delta E^{\rm pert}_{\rm tot}$	−0.165	−0.100	−0.095	−0.057
$\Delta E^{\rm pert}_{\rm kin}$	−0.348	−0.276	−0.198	−0.155

In perturbative calculations, the changes in particle energy $\Delta E^{\rm pert}_{\rm part}$ can be easily related to the energy splitting $\Delta E_{\rm split}$ between the blocked state and its unoccupied time-reversal counterpart through $\Delta E^{\rm pert}_{\rm part} \approx -\frac{1}{2}\Delta E_{\rm split}$, as the sum over the energies of other occupied single-particle states is the same in calculations with and without NM because the polarization effects are absent (Sec. IV B). Energy splittings between different signatures of the blocked [330]1/2 state are $\Delta E_{\rm split} = 0.653$ MeV and $\Delta E_{\rm split} = 0.476$ MeV for odd-neutron (^{31}S) and odd-proton (^{31}P) nuclei, respectively. This result clearly indicates that the contributions of the Coulomb force to the proton single-particle energies in the presence of NM are at the origin of the fact that additional binding owing to NM is smaller for odd-proton nuclei compared with odd-neutron ones. Analysis of ^{33}S and ^{33}Cl leads to the same conclusions.

The situation is more complicated in odd-odd nuclei (^{30}P and ^{34}Cl), in which considerable energy splitting between the $r = +1$ and the $r = -1$ configurations is obtained in the calculations. The microscopic mechanism of binding modifications is illustrated in Table IV on the example of configurations A and B of ^{34}Cl.

NM provides additional binding of about 0.4 MeV in configuration A, which has signature $r = -1$. In this configuration, proton and neutron currents owing to the occupation of proton and neutron $5/2[202]^-$ states are in the same direction, which results in an appreciable total baryonic current. This baryonic current leads to sizable modifications in the $E_{\rm part}$, E_σ, $E^{\rm TL}_{\omega}$, and $E^{\rm SL}_{\omega}$ terms (Table IV). These are precisely the same

TABLE IV. Changes $\Delta E_i = E^{\rm NM}_i - E^{\rm WNM}_i$ in different terms of the total energy [Eq. (15)] in the SD configurations $A \equiv \pi[202]5/2^- \otimes \nu[202]5/2^-$ ($r = -1$) and $B \equiv \pi[202]5/2^+ \otimes \nu[202]5/2^-$ ($r = +1$) of ^{34}Cl induced by NM [columns (3)–(6)]. Column (2) lists the absolute energies (MeV) of different energy terms in the case where NM is neglected. Configurations are given with respect to the doubly magic SD configuration of ^{32}S. Fully self-consistent [columns (2), (3), and (5)] and perturbative [columns (4) and (6)] results are presented.

Quantity (1)	$E^{\rm WNM}_i$(A, B) (2)	ΔE_i(A) (3)	$\Delta E^{\rm pert}_i$(A) (4)	ΔE_i(B) (5)	$\Delta E^{\rm pert}_i$(B) (6)
$E_{\rm part}$	−835.845	−1.471	−0.791	−0.004	−0.003
E_σ	−4415.660	−7.862		+0.004	
$E_{\sigma{\rm NL}}$	84.884	−0.036		−0.001	
$E^{\rm TL}_{\omega}$	3698.240	7.126		−0.003	
$E^{\rm SL}_{\omega}$	0.0	−0.414	−0.414	0.0	−0.001
$E^{\rm TL}_{\rho}$	0.061	0.0		0.0	
$E^{\rm SL}_{\rho}$	0.0	0.0		−0.043	−0.043
$E_{\rm Coul}$	59.832	0.052	0.025	−0.002	−0.003
$E_{\rm cm}$	−9.492	0.0		0.0	
$E_{\rm tot}$	−272.693	−0.376	−0.402	0.041	0.043
$E_{\rm kin}$	479.210	−0.103	−0.841	−0.002	0.003

terms that are strongly affected by NM in odd-mass nuclei; see Sec. IV B. The fermionic contribution to $E^{\rm NM} - E^{\rm WNM}$ (the $\Delta E_{\rm part}$ term) is defined by more or less equal contributions from time-odd mean fields and polarization effects in time-even mean fields. On the contrary, time-odd mean fields define only approximately one-third ($\Delta E^{\rm SL}_{\omega} = -0.413$ MeV) of the mesonic contribution to $E^{\rm NM} - E^{\rm WNM}$, whereas the rest is caused by the polarization effects in time-even mean fields (the ΔE_{σ} and ΔE^{T}_{ω} terms).

NM leads to the loss of binding in configuration B, which has $r = +1$. In this configuration, the proton and neutron currents owing to the $\pi[202]5/2^+$ and $\nu[202]5/2^-$ states are in opposite directions, so the total baryonic current is very close to zero. As a result, the impact of NM is close to zero for the majority of terms in Eq. (15) (see Table IV). The only exception is the $E^{\rm SL}_{\rho}$ term, which represents the space-like component of the isovector-vector ρ field. This term depends on the difference of proton and neutron currents [Eq. (22)], which, for the present case of opposite currents, gives a nonzero result. As follows from Table IV, this term is predominantly responsible for the loss of binding owing to NM in configuration B.

It is well known that many physical quantities are additive in calculations without pairing (see Ref. [33] and references therein). The additivity principle states that the average value of a one-body operator $\hat{O}$ in a given many-body configuration k, $O(k)$, relative to the average value in the core configuration, $O^{\rm core}$, is equal to the sum of the effective contributions $o^{\rm eff}_{\alpha}$ of the particle and hole states by which the kth configuration differs from that of the core [33],

$$\delta O(k) = O(k) - O^{\rm core} = \sum_{\alpha} c_{\alpha}(k) o^{\rm eff}_{\alpha}. \qquad (35)$$

Coefficients $c_{\alpha}(k)$ $[c_{\alpha}(k) = 0, \text{or} + 1, \text{or} - 1]$ define the single-particle content of configuration k with respect to the core configuration (see Ref. [33] for details). Let us check whether additional binding owing to NM (the $\Delta E_{\rm tot} = E^{\rm NM} - E^{\rm WNM}$ quantity) is additive. The doubly magic SD configuration $\pi 3^2 \nu 3^2$ in the even-even ^{32}S nucleus is used as a core for this analysis: The effective contributions $\delta E^{\rm eff}_i$ of the particle state(s) to $\Delta E_{\rm tot}$ are given by $\delta E^{\rm eff}_i = [E_i(\text{nucleus A}) - E_i(\text{core})]^{\rm NM} - [E_i(\text{nucleus A}) - E_i(\text{core})]^{\rm WNM} = E^{\rm NM}_i(\text{nucleus A}) - E^{\rm WNM}_i(\text{nucleus A}) = \Delta E_i(\text{nucleus A})$ because the core configuration is not affected by NM. Thus, the additivity implies that $\Delta E_{\rm tot}[^{34}\text{Cl}(r = +1)] = \Delta E_{\rm tot}(^{33}\text{S}) + \Delta E_{\rm tot}(^{33}\text{Cl})$ $\{\Delta E_{\rm tot}[^{34}\text{Cl}(r = -1)] = \Delta E_{\rm tot}(^{33}\text{S}) - \Delta E_{\rm tot}(^{33}\text{Cl})\}$ for the situation when the proton and neutron currents in ^{34}Cl are in the same (opposite) directions. Figure 16 clearly shows that additivity conditions are not fulfilled and that additional binding owing to NM is not additive in self-consistent calculations. The analysis involving odd-odd ^{30}P and odd ^{31}P, ^{31}S nuclei leads to the same conclusion (see Fig. 16).

The additivity is also violated in perturbative calculations: Comparison of Tables III [columns (4) and (5)] and IV [columns (4) and (6)] reveals that the conditions $\Delta E^{\rm pert}_i[^{34}\text{Cl}(r = \pm 1)] = \Delta E^{\rm pert}_i(^{33}\text{S}) \pm \Delta E^{\rm pert}_i(^{33}\text{Cl})$ are violated both for the total energy (i = tot) and for the individual components of the total energy (i = part, $^{\rm SL}_{\omega}$, $^{\rm SL}_{\rho}$, Coul). The analysis of $\Delta E^{\rm pert}_{\rm part}$ (this term provides the largest contribution to $\Delta E^{\rm pert}_{\rm tot}$; see Tables III and IV) allows understanding of the origin of the violation of additivity for the $\Delta E^{\rm pert}_{\rm tot}$ quantity. In the odd-proton ^{31}Cl nucleus, $\Delta E^{p[\rm pert]}_{\rm part} \approx -\frac{1}{2}\Delta E^{p}_{\rm split}$ ($\Delta E^{p}_{\rm split}$ is the energy splitting between the blocked proton state and its signature counterpart) and $\Delta E^{p}_{\rm split}$ depends predominantly on the proton current induced by the odd proton. The same is true in the odd-neutron ^{33}S nucleus, where $\Delta E^{n}_{\rm split}$ depends predominantly on the neutron current induced by the odd neutron. Additivity principle implies $\Delta E^{\rm odd-odd[pert]}_{\rm part} \approx -\frac{1}{2}\Delta E^{p}_{\rm split} + \frac{1}{2}\Delta E^{n}_{\rm split}$ for the ^{34}Cl$(r = +1)$ configuration, in which the proton and neutron currents are in the same direction. However, proton $\Delta E^{p[\rm odd-odd]}_{\rm split}$ (neutron $\Delta E^{n[\rm odd-odd]}_{\rm split}$) energy splitting between the blocked proton (neutron) state and its time-reversal counterpart in odd-odd nuclei depends on the total baryonic (proton + neutron) current in this configuration. On the contrary, the additivity principle implies that these proton and neutron quantities depend on the individual proton and neutron currents in the odd-odd nucleus, respectively. This total current is approximately two times stronger than the individual (proton or neutron) currents in odd-mass nuclei. As a consequence, the $\Delta E^{p[\rm odd-odd]}_{\rm split}$ and $\Delta E^{n[\rm odd-odd]}_{\rm split}$ values in the odd-odd mass nucleus are larger than the same quantities ($\Delta E^{p}_{\rm split}$ and $\Delta E^{n}_{\rm split}$) in odd-mass nuclei by a factor of close to 2. As a result, $\Delta E^{\rm pert}_{\rm part}[^{34}\text{Cl}(r = +1)] \approx 2[\Delta E^{\rm pert}_{\rm part}(^{33}\text{S}) + \Delta E^{\rm pert}_{\rm part}(^{33}\text{Cl})]$ (see Tables III and IV), which clearly indicates the violation of additivity for the $\Delta E^{\rm pert}_{\rm part}$ quantity (and for the $\Delta E^{\rm pert}_{\rm tot}$ quantity).

Figure 16 also shows the results for the four-particle excited SD states $\pi(\text{ab}) \otimes \nu(\text{ab})$ in ^{32}S, for which the calculated rotational structures display the signature separation induced by time-odd mean fields [64,73]. These configurations are formed by exciting proton and neutron from the $[330]1/2^-$ orbitals below the $N = 16$ and $Z = 16$ SD shell gaps into the $[202]5/2^{\pm}$ orbitals located above these gaps. They have the $\pi 3^1 \nu 3^1$ structure in terms of intruder orbitals. When NM is neglected these four configurations are degenerated in energy. This degeneracy is broken and additional binding, which depends on the total signature of the configuration (0.907 MeV for $r = +1$ configurations and 0.468 MeV for $r = -1$ configurations in calculations with the NL3 parametrization), is obtained when NM is taken into account. The NL1 and NLSH parametrizations of the RMF Lagrangian give very similar values for additional binding owing to NM. The essential difference between the relativistic and the nonrelativistic calculations lies in (i) the size of the energy gap between the $r = +1$ and the $r = -1$ configurations and (ii) the impact of time-odd mean fields on the energy of the $r = -1$ states. This energy gap is about 2 MeV in the Skyrme EDF calculations with the SLy4 force [73], whereas it is much smaller, around 0.45 MeV, in CRMF calculations with the NL1, NL3, and NLSH parametrizations. The energies of the $r = -1$ states are not affected by time-odd mean fields in the Skyrme EDF calculations [73], whereas appreciable additional binding is generated by NM for these states in CRMF calculations (Fig. 16).

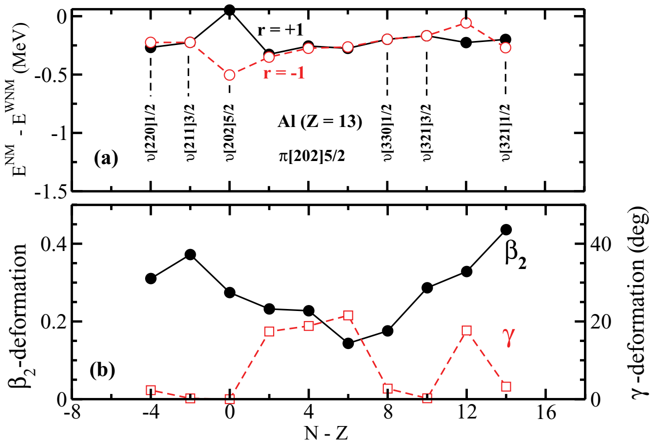

FIG. 17. (Color online) Impact of NM on binding energies of the lowest configurations in odd-odd Al nuclei. (a) The $E^{\mathrm{NM}} - E^{\mathrm{WNM}}$ quantity for different signatures. Structures of the blocked states are shown by the Nilsson labels only in cases where the configurations are near-prolate. The same state is blocked in the proton subsystem of all nuclei. (b) The β_2 and γ deformations of the configurations under study.

Figures 17 and 18 show the results of the calculations for ground-state configurations in odd-odd Al and Cl nuclei. The calculations suggest that signature separation owing to time-odd mean fields is also expected in the configurations of odd-odd nuclei located at zero or low excitation energies. The signature separation is especially pronounced in $N = Z$ ^{26}Al (the $\pi[202]5/2 \otimes \nu[202]5/2$ configuration) and ^{34}Cl nuclei. This is because proton and neutron currents in these configurations are almost the same both in strength and in spatial distribution. As a result, their contribution to the total energy is large when these currents are in the same direction ($r = -1$ configurations) and close to zero when these currents are in opposite directions ($r = +1$ configurations). Note that ^{26}Al is axially deformed, whereas ^{34}Cl is triaxially deformed, with $\gamma \sim 30^\circ$. However, both of them show enhancement of the signature separation at $N = Z$.

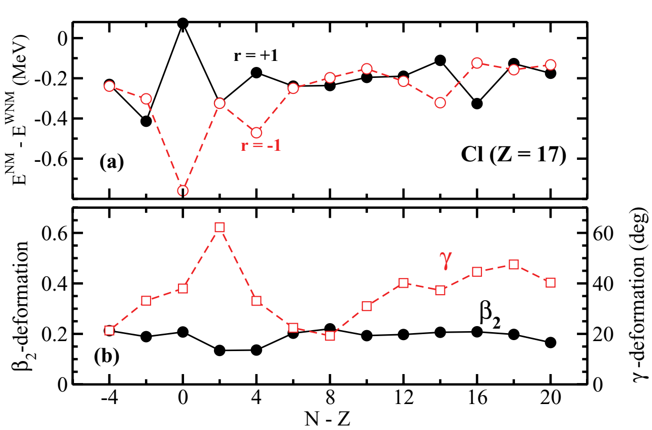

FIG. 18. (Color online) The same as Fig. 17 but for the lowest configurations in odd-odd Cl nuclei.

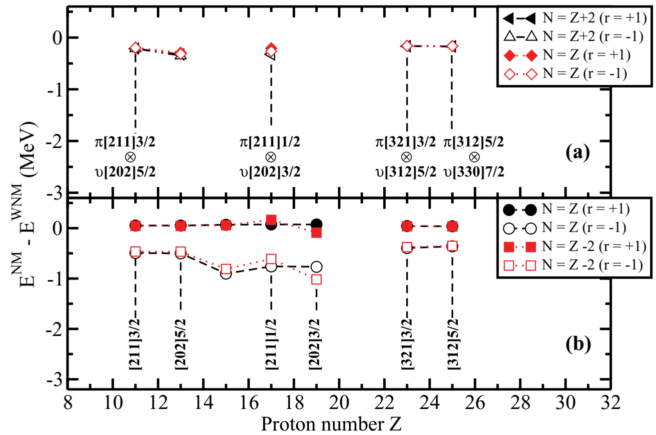

FIG. 19. (Color online) Impact of NM on binding energies of the configurations in odd-odd nuclei in the vicinity of the $N = Z$ line as a function of proton number Z. (a) Results for configurations with different blocked proton and neutron states; (b) results for configurations with the same blocked proton and neutron states. Structures of the blocked states are shown by the Nilsson labels only in cases where the configurations are near-prolate. Note that in (b), only one Nilsson label is shown, as the blocked proton and neutron states have the same structure. Results are shown only in cases where convergence has been achieved for both $N = Z$ and $N = Z - 2$ (or $N = Z + 2$) nuclei.

The signature separation is rather small for the majority of nuclei away from the $N = Z$ line. This is a consequence of the fact that the strength of the currents in one subsystem (and thus the impact of NM on binding energies) is much stronger than that in another subsystem. As a result, there is no big difference (large signature separation) between the cases in which proton and neutron currents are in the same and opposite directions. However, some nuclei away from the $N = Z$ line also show appreciable signature separation. These are ^{38}Al and ^{38,48,50}Cl nuclei (Figs. 17 and 18), for which the strengths of proton and neutron currents (but not necessarily the spatial distribution of the currents) are of the same order of magnitude.

It was suggested in Ref. [30] that the effects of time-odd mean fields are enhanced at the $N = Z$ line. However, Fig. 19 clearly shows that the enhancement of signature separation is not restricted to the $N = Z$ line. Indeed, signature separation of the configurations based on the same combination of blocked proton and neutron states are very similar in $N = Z$ and $N = Z \pm 2$ nuclei despite the fact that the deformations of compared nuclei sometimes differ appreciably. There is considerable signature separation in the configurations based on the same blocked proton and neutron states in $N = Z$ and $N = Z - 2$ nuclei [Fig. (19b)]. On the other hand, almost no signature splitting is observed in $N = Z$ and $N = Z + 2$ nuclei when the configurations are based on different blocked proton and neutron states [Fig. 19(a)]. This suggests that the enhancement of signature splitting is due to similar proton and neutron current distributions (see discussion in previous paragraph).

When considering odd-odd nuclei one has to keep in mind that the present approach takes into account only the portion of the correlations between the blocked proton and neutron and neglects the pairing. In particular, the residual interaction of the unpaired proton and neutron leading to Gallagher-Moshkowski doublets of two-quasiparticle states with $K_> = \Omega_p + \Omega_n$ and $K_< = |\Omega_p - \Omega_n|$ [74,75] is not taken into account. Thus, future development of the model is required to compare the experimental data on odd-odd nuclei directly with calculations. This question is discussed in more detail in the companion paper [36].

VII. CONCLUSIONS

Time-odd mean fields (nuclear magnetism) have been studied at no rotation in a systematic way within the framework of CDFT by blocking the single-particle states with a fixed signature. The main results can be summarized as follows.

(i) In odd-mass nuclei, nuclear magnetism always leads to an additional binding, indicating its attractive nature in the CDFT. This additional binding only weakly depends on the parametrization of the RMF Lagrangian. On the contrary, time-odd mean fields in Skyrme EDF can be attractive and repulsive and show considerable dependence on the parametrization of the density functional. This additional binding is larger in odd-neutron states than in odd-proton ones in the CDFT framework. The underlying microscopic mechanism of additional binding owing to NM has been studied in detail. The perturbative results clearly indicate that additional binding owing to NM is defined mainly by time-odd fields and that the polarization effects in fermionic and mesonic sectors of the model cancel each other to a large degree.

(ii) Additional binding owing to NM can have a profound effect on the properties of odd-proton nuclei in the ground and excited states in the vicinity of the proton drip line. In some cases it can transform a nucleus that is proton unbound (in calculations without NM) into a nucleus that is proton bound. This additional binding can significantly affect the decay properties of proton-unbound nuclei by (i) increasing the half-lives of proton emitters (by many orders of magnitude in light nuclei) or (ii) moving the Q_p value inside or outside the Q_p window favorable for experimental observation of proton emission.

(iii) Relative energies of different (quasi)particle states in medium- and heavy-mass nuclei are only weakly affected by time-odd mean fields. This is because additional bindings owing to NM show little dependence on the blocked single-particle state. As a result, the present investigation suggests that time-odd mean fields can be neglected in the fits of CDFs aimed at accurate description of the energies of single-particle states.

(iv) The phenomenon of signature separation [73] and its microscopic mechanism have been investigated in detail. It is shown that this phenomenon is active also in the configurations of odd-odd nuclei. It is enhanced for configurations having the same blocked proton and neutron states; this takes place either at ground state or at low excitation energy in nuclei at or close to the $N = Z$ line. Some configurations away from the $N = Z$ line also show this effect but the signature separation is appreciably smaller.

The present investigation has focused on the study of time-odd mean fields in the CDFT with nonlinear parametrizations of the Lagrangian. Point coupling [76] and density-dependent meson-nucleon coupling [56] models are other classes of CDF theories. It is important to compare them to make significant progress toward a better understanding of time-odd mean fields. Work in this direction is in progress, and the results will be presented in the forthcoming companion article [36].

ACKNOWLEDGMENTS

The private communication of P. Ring [58] is greatly appreciated. The material is based on work supported by the Department of Energy under Grant No. DE-FG02-07ER41459.

[1] R. J. Furnstahl and B. D. Serot, Nucl. Phys. **A673**, 298 (2000).

[2] G. Lalazissis, P. Ring, and D. Vretenar, eds., *Extended Density Functionals in Nuclear Structure Physics*. Springer Lecture Notes in Physics, Vol. 641 (Springer, Berlin, 2004).

[3] R. J. Furnstahl, Proceedings of the ECT* school on "Renormalization Group and Effective Field Theory Approaches to Many-Body Systems." Springer Lecture Notes in Physics, in press. arXiv:0708.1602 at xxx.lanl.gov.

[4] R. J. Furnstahl, G. Rupak, and T. Schäfer, Annu. Rev. Nucl. Part. Sci. **58**, 1 (2008).

[5] P. Hohenberg and W. Kohn, Phys. Rev. **136**, B864 (1964).

[6] W. Kohn and L. J. Sham, Phys. Rev. **140**, A1133 (1965).

[7] W. Kohn, Rev. Mod. Phys. **71**, 1253 (1999).

[8] R. M. Dreizler and E. K. U. Gross, *Density Functional Theory* (Springer-Verlag, Berlin, 1990).

[9] B. D. Serot and J. D. Walecka, Int. J. Mod. Phys. E **6**, 515 (1997).

[10] M. Bender, P.-H. Heenen, and P.-G. Reinhard, Rev. Mod. Phys. **75**, 121 (2003).

[11] D. Vretenar, A. V. Afanasjev, G. A. Lalazissis, and P. Ring, Phys. Rep. **409**, 101 (2005).

[12] B. G. Carlsson, J. Dobaczewski, and M. Kortelainen, Phys. Rev. C **78**, 044326 (2008).

[13] A. Sobiczewski and K. Pomorski, Prog. Part. Nucl. Phys. **58**, 292 (2007).

[14] P. Ring and P. Schuck, *The Nuclear Many-Body Problem* (Springer-Verlag, Berlin, 2000).

[15] B. B. Serot and J. D. Walecka, Adv. Nucl. Phys. **16**, 1 (1986).

[16] R. J. Furnstahl and B. D. Serot, Nucl. Phys. **A671**, 447 (2000).

[17] J. Dobaczewski and J. Dudek, Phys. Rev. C **52**, 1827 (1995).

[18] A. V. Afanasjev and P. Ring, Phys. Rev. C **62**, 031302(R) (2000).

[19] U. Post, E. Wüst, and U. Mosel, Nucl. Phys. **A437**, 274 (1985).

[20] W. Koepf and P. Ring, Nucl. Phys. **A511**, 279 (1990).

[21] J. König and P. Ring, Phys. Rev. Lett. **71**, 3079 (1993).

[22] H. Zduńczuk, W. Satula, and R. A. Wyss, Phys. Rev. C **71**, 024305 (2005).

[23] A. V. Afanasjev, Phys. Rev. C **78**, 054303 (2008).

[24] U. Hofmann and P. Ring, Phys. Lett. **B214**, 307 (1988).

[25] Y. M. Engel, D. M. Brink, K. Geoke, S. J. Krieger, and D. Vauterin, Nucl. Phys. **A249**, 215 (1975).
[26] V. O. Nesterenko, W. Kleinig, J. Kvasil, P. Vesely, and P.-G. Reinhard, Int. J. Mod. Phys. E **17**, 89 (2008).
[27] N. Hinohara, T. Nakatsukasa, M. Matsuo, and K. Matsuyanagi, Prog. Theor. Phys. **115**, 567 (2006).
[28] A. S. Umar and V. E. Oberacker, Phys. Rev. C **73**, 054607 (2006).
[29] M. Bender, J. Dobaczewski, J. Engel, and W. Nazarewicz, Phys. Rev. C **65**, 054322 (2002).
[30] W. Satula, in *Nuclear Structure 98*, edited by C. Baktash. AIP Conf. Proc. No. 481 (AIP, New York, 1999), p. 114.
[31] T. Duguet, P. Bonche, P.-H. Heenen, and J. Meyer, Phys. Rev. C **65**, 014310 (2001).
[32] A. V. Afanasjev, T. L. Khoo, S. Frauendorf, G. A. Lalazissis, and I. Ahmad, Phys. Rev. C **67**, 024309 (2003).
[33] M. Matev, A. V. Afanasjev, J. Dobaczewski, G. A. Lalazissis, and W. Nazarewicz, Phys. Rev. C **76**, 034304 (2007).
[34] J. Dobaczewski, J. Dudek, and R. Wyss, Phys. Rev. C **67**, 034308 (2003).
[35] K. Rutz, M. Bender, P.-G. Reinhard, and J. A. Maruhn, Phys. Lett. **B468**, 1 (1999).
[36] A. V. Afanasjev and H. Abusara (in preparation).
[37] W. Koepf and P. Ring, Nucl. Phys. **A493**, 61 (1989).
[38] A. V. Afanasjev, J. König, and P. Ring, Nucl. Phys. **A608**, 107 (1996).
[39] A. V. Afanasjev and H. Abusara, Phys. Rev. C **78**, 014315 (2008).
[40] P.-G. Reinhard, M. Rufa, J. Maruhn, W. Greiner, and J. Friedrich, Z. Phys. A **323**, 13 (1986).
[41] W. Greiner, *Relativistic Quantum Mechanics* (Springer-Verlag, Berlin, 1990).
[42] G. A. Lalazissis, J. König, and P. Ring, Phys. Rev. C **55**, 540 (1997).
[43] G. A. Lalazissis, S. Karatzikos, R. Fossion, D. Pena Arteaga, A. V. Afanasjev, and P. Ring, Phys. Lett. **B671**, 36 (2009).
[44] M. Rufa, P.-G. Reinhard, J. A. Maruhn, W. Greiner, and M. R. Strayer, Phys. Rev. C **38**, 390 (1988).
[45] M. Bender, K. Rutz, P.-G. Reinhard, J. A. Maruhn, and W. Greiner, Phys. Rev. C **60**, 034304 (1999).
[46] M. Rashdan, Phys. Rev. C **63**, 044303 (2001).
[47] M. M. Sharma, M. A. Nagarajan, and P. Ring, Phys. Lett. **B312**, 377 (1993).
[48] W. Long, J. Meng, N. Van Giai, and S. Zhou, Phys. Rev. C **69**, 034319 (2004).
[49] Z. Ren and H. Toki, Nucl. Phys. **A689**, 691 (2001).
[50] R. Brockmann and H. Toki, Phys. Rev. Lett. **68**, 3408 (1992).
[51] M. M. Sharma, Phys. Lett. **B666**, 140 (2008).
[52] B. G. Todd-Rutel and J. Piekarewicz, Phys. Rev. Lett. **95**, 122501 (2005).
[53] R. Kumar, B. K. Agrawal, and S. K. Dhiman, Phys. Rev. C **74**, 034323 (2006).
[54] S. Typel and H. H. Wolter, Nucl. Phys. **A656**, 331 (1999).
[55] T. Niksić, D. Vretenar, P. Finelli, and P. Ring, Phys. Rev. C **66**, 024306 (2002).
[56] G. A. Lalazissis, T. Niksić, D. Vretenar, and P. Ring, Phys. Rev. C **71**, 024312 (2005).
[57] P. Ring, Y. K. Gambhir, and G. A. Lalazissis, Comput. Phys. Commun. **105**, 77 (1997).
[58] P. Ring (private communication).
[59] M. Yamagami and K. Matsuyanagi, Nucl. Phys. **A672**, 123 (2000).
[60] K. Langanke and M. Wiescher, Rep. Prog. Phys. **64**, 1657 (2001).
[61] J. Rikovska Stone, J. Phys. G **31**, R211 (2005).
[62] M. Zalewski, J. Dobaczewski, W. Satula, and T. R. Werner, Phys. Rev. C **77**, 024316 (2008).
[63] K. Rutz, M. Bender, P.-G. Reinhard, J. A. Maruhn, and W. Greiner, Nucl. Phys. **A634**, 67 (1998).
[64] A. V. Afanasjev, P. Ring, and I. Ragnarsson, in *International Workshop PINGST, 2000 Selected Topics on $N = Z$ Nuclei, 2000, Lund, Sweden*, edited by D. Rudolph and M. Hellström (Bloms i Lund AB, Lund, Sweden, 2000), p. 183.
[65] A. V. Afanasjev, P. Ring, and J. König, Nucl. Phys. **A676**, 196 (2000).
[66] J. Dobaczewski, P. Magierski, W. Nazarewicz, W. Satula, and Z. Szymański, Phys. Rev. C **63**, 024308 (2001).
[67] G. F. Bertsch, C. A. Bertulani, W. Nazarewicz, N. Schunck, and M. V. Stoitsov, Phys. Rev. C **79**, 034306 (2009).
[68] T. Duguet, P. Bonche, P.-H. Heenen, and J. Meyer, Phys. Rev. C **65**, 014311 (2001).
[69] P. J. Woods and C. N. Davids, Annu. Rev. Nucl. Part. Sci. **47**, 541 (1997).
[70] S. Åberg, P. B. Semmes, and W. Nazarewicz, Phys. Rev. C **56**, 1762 (1997).
[71] G. A. Lalazissis, D. Vretenar, and P. Ring, Nucl. Phys. **A679**, 481 (2001).
[72] V. I. Goldansky, Nucl. Phys. **19**, 482 (1960).
[73] H. Molique, J. Dobaczewski, and J. Dudek, Phys. Rev. C **61**, 044304 (2000).
[74] C. J. Gallagher Jr., and S. A. Moszkowski, Phys. Rev. **111**, 1282 (1958).
[75] J. P. Boisson, R. Piepenbring, and W. Ogle, Phys. Rep. **26**, 99 (1976).
[76] T. Bürvenich, D. G. Madland, J. A. Maruhn, and P.-G. Reinhard, Phys. Rev. C **65**, 044308 (2002).
[77] Z. Szymanski, *Fast Nuclear Rotations*. Oxford Studies in Physics (Clarendon Press, Oxford, 1983).